Journal of Structural Geology 32 (2010) 445–463

Contents lists available at ScienceDirect

Journal of Structural Geology

journal homepage: www.elsevier.com/locate/jsg

Structure, kinematics and ages of transpression during strain-partitioning in the Chongshan shear zone, western Yunnan, China

Bo Zhang [a,*], Jinjiang Zhang [a], Dalai Zhong [b]

[a] The Key Laboratory of Orogenic Belts and Crustal Evolution, Department of Geology, Peking University, Beijing 100871, China
[b] Institute of Geology and Geophysics, Chinese Academy of Sciences, Beijing 100029, China

ARTICLE INFO

Article history:
Received 15 June 2009
Received in revised form
4 February 2010
Accepted 15 February 2010
Available online 21 February 2010

Keywords:
Kinematics
Geochronology
Transpression
Chongshan shear zone
Western Yunnan

ABSTRACT

The Chongshan shear zone extends from the eastern Himalayan Syntaxis to the Lincang Granitic pluton in Yunnan Province, China. The structure and kinematics show that the shear zone comprises mainly of mylonitic gneiss–migmatite and schist with a dextral-dominated strike-slip motion in an N–S trending northern segment, and a sinistral strike-slip shear in NW–SE trending middle and southern segments. Both were developed under a bulk, regional-scale sinistral transpression. SHRIMP and LA-ICPMS U–Pb and $^{40}Ar/^{39}Ar$ dating reveal two Tertiary magmatic events along the zone, followed by younger sinistral strike-slip shear. The Eocene magmatic event (c. 55–38 Ma), followed by metamorphism at c. 36 Ma, happened before the strike-slip motion. The strike-slip shear along the zone began c. 32 Ma, which generated shear heating from 32 to 22 Ma. The $^{40}Ar/^{39}Ar$ ages of syn-kinematic micas, range from 19 to 14 Ma, and indicate that the strike-slip shear continued to this time with coeval transpressional exhumation and uplift of the metamorphic rocks along the Biluoxueshan–Chongshan chain. The Chongshan zone is thus a Cenozoic shear zone, which was contemporaneous with motion on the left-lateral Ailao Shan-Red River shear zone and the right-lateral Gaoligong shear zone, and should be important in accommodating the northwards movement of India during collision. During Oligocene to Miocene times, the continental block that was extruded between the Ailao Shan-Red River and Gaoligong shear zones was dismembered into at least two major fragments by the Chongshan shear zone.

1. Introduction

Following the India–Asia collision at equatorial latitudes approximately since 54–49 Ma (Dewey et al., 1989; Zhu et al., 2005a), India has indented into the Asian continent c. 2000 km northwards, forming the Himalayan orogen, crustal thickening and the uplift of the Tibetan plateau (e.g. Searle et al., 2007). Related to this collision, widespread intra-continental deformation occurred in SE Asia along large-scale NW–SE trending strike-slip shear zones (Tapponnier et al., 1982, 1986; Peltzer and Tapponnier, 1988). Abundant geological and geochronological evidence implies that the Ailao Shan-Red River shear zone in southern China and Vietnam, the Wang Chao (or Mae Ping) and Three Pagadas strike-slip fault zones in northern Thailand, the Gaoligong shear zone and Sagaing fault in southern China and Burma all played a key role in the eastward movement of fault-bounded continental blocks during the northward indentation of the Indian continent (Tapponnier et al., 1986; Leloup et al., 1995, 2007; Lacassin et al., 1997; Wang and Burchfiel, 1997; Morley et al., 2001; Morley, 2002; Gilley et al., 2003).

The Chongshan shear zone (Fig. 1), also referred as the Chongshan metamorphic zone because of the good outcrops of metamorphic and intrusive rocks, extends from the eastern Himalayan Syntaxis in the north, then along the Biluoxueshan–Chongshan mountain to the south, and finally converges with the Lincang Granite pluton in the south (Fig. 2; BGMRYP, 1987, 1990; Wang and Burchfiel, 1997; Akciz et al., 2008). This zone marks the boundary between the Lanping-Simao terrane in the east and the Shan-Thai block (Subimasu) in the west (Fig. 2), a topographic high extending into Thailand (Morley, 2004; Searle et al., 2007). Metamorphic rocks exposed in this zone include mica schists, gneisses, marbles and quartzites with metamorphic grades ranging from greenschist to high-amphibolite facies, some of these rocks have been suggested to be Precambrian basement (BGMRYP, 1987; Heppe et al., 2007). Although the Chongshan shear zone is an important geological boundary, the structure, kinematics and geochronology along it have not been constrained very well other than a recently proposed early Cenozoic strike-slip shear event by Akciz et al. (2008). Other

* Corresponding author. Tel.: +86 10 62758325.
E-mail address: geozhangbo@pku.edu.cn (B. Zhang).

0191-8141/$ – see front matter © 2010 Elsevier Ltd. All rights reserved.
doi:10.1016/j.jsg.2010.02.001

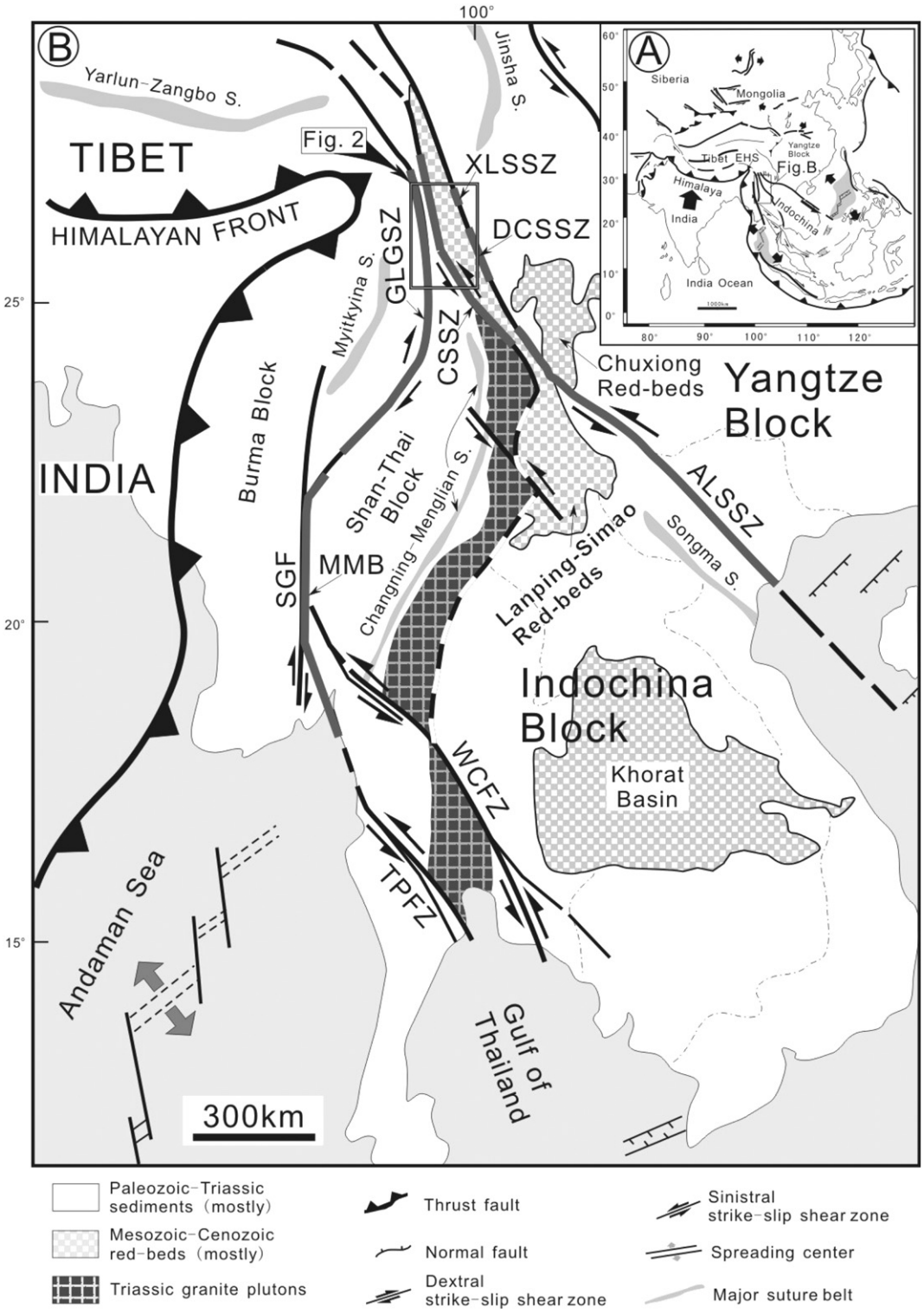

Fig. 1. Schematic tectonic map of SE Asia showing major fault and shear zones. Inset (A) shows the extrusion of Indochina in response to northward penetration by India (modified after Peltzer and Tapponnier, 1988; Tapponnier et al., 1990; Leloup et al., 1995; Morley et al., 2001; Morley, 2007). (B) CSSZ, Chongshan shear zone; Xuelongshan shear zone (XLSSZ), Diancangshan shear zone (DCSSZ) and Ailao Shan shear zone (ALSSZ) belong to the Ailao Shan-Red River shear zone; EHS, Eastern Himalayan Syntaxis; WCFZ, Wang Chao fault zone; TPF, three Pagodas fault zone; SGF, Sagaing fault; MMB, Mogok metamorphic zone.

recent geochronological analyses on the southern Chongshan mountain also revealed some Cenozoic events (Wang et al., 2006; Heppe et al., 2007). In order to get a better understanding of this poorly documented zone, we conducted a detailed study between latitudes 24°–28° north and longitudes 99°– 100° east (Fig. 1).

We have carried out a structural and kinematic study along the Chongshan shear zone and across three sections in western Yunnan, China (Fig. 2). We also present sensitive high resolution ion microprobe (SHRIMP) and laser ablation-multi-collector-inductively coupled plasma mass spectrometer (LA-ICPMS)

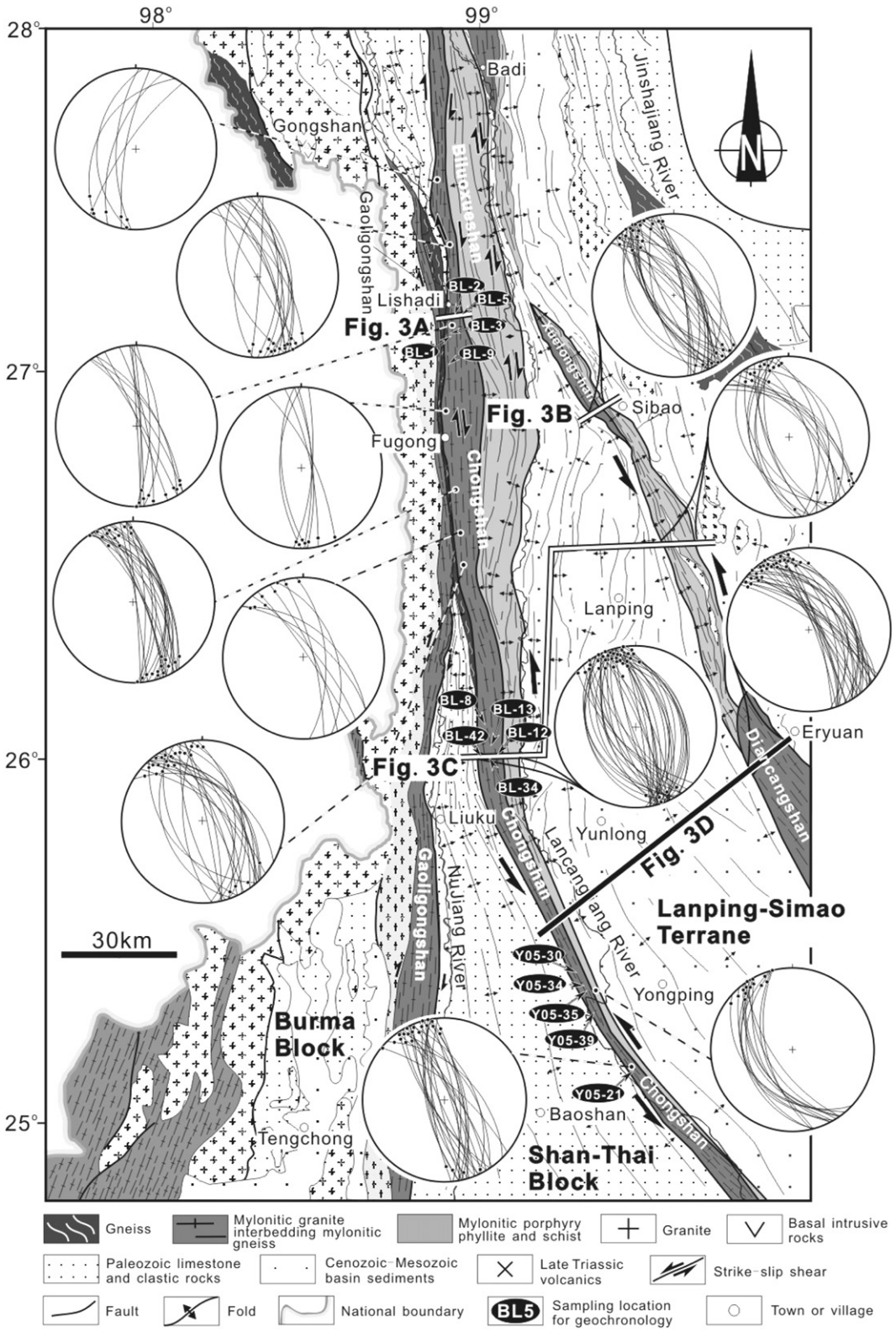

Fig. 2. Simplified geological map of the Chongshan shear zone and adjacent areas, showing stereograms of the foliation (large circle) and mineral stretching lineation (black dot) for observing sites along the Chongshan and Ailao Shan-Red River shear zones. All diagrams are equal-area Schmidt net, lower hemisphere.

geochronological data to constrain the ages of magmatism, deformation and metamorphism in the zone. $^{40}Ar/^{39}Ar$ dating was also carried out to constrain the end of shearing and associated retrograde metamorphism along the zone. Combining these data with structure analysis, we then compare the tectonic evolution of the Chongshan shear zone and assess its relationship to other major strike-slip shear zones in the region.

2. Geological setting

The Yunnan–Myanmar area comprises a triangular region of crust bounded on its western margin by the N–S striking Gaoligong shear zone and NNE-striking Sagaing fault, and on its eastern side by the NW-SE striking Ailao Shan-Red River shear zone (Fig. 1). The area is characterized by prominent, young strike-slip shear zones and faults (Zhong and Tapponnier, 1990; Leloup et al., 1995; Morley, 2007). From west to east these are: the Gaoligong; Chongshan and Ailao Shan-Red River shear zones. The Gaoligong shear zone separates the Burma and Shan-Thai blocks, and the Chongshan shear zone lies between the Shan-Thai block and Lanping-Simao terrane (Fig. 2).

The Gaoligong shear zone extends southward from the eastern Himalayan Syntaxis to the eastern Tengchong area and then swings northeastward to join the Sagaing fault (Figs. 1 and 2). The zone is exposed completely along the Gaoligong mountain west of the Nujiang valley (Figs. 1 and 2; Wang and Burchfiel, 1997; Zhong, 2000) where dextral ductile shear sense indicators are widely preserved. The zone is thought to form the western boundary of an extruded Indochina continental fragment (Ji et al., 2000; Wang et al., 2006; Akciz et al., 2008; Lin et al., 2009). Wang et al. (2006) stated that dextral strike-slip motions on the Gaoligong shear zone began at 32 Ma based on the $^{40}Ar/^{39}Ar$ dating of syn-kinematic minerals. However, Ji et al. (2000) dated syn-kinematic muscovites and hornblendes and found two peak deformation ages between 24–19 Ma and 14–11 Ma within the southern segment of the zone exhibiting dextral strike-slip. More recently, the main phase of dextral strike-slip shearing along the northern extension of the Gaoligong zone into the Jiali fault has been dated between 18 and 13 Ma (Lin et al., 2009).

The Chongshan shear zone forms the over 250-km long boundary between the Lanping-Simao terrane and Shan-Thai block (Fig. 1B). This zone consists mainly of mylonitic gneisses with amphibolite enclaves, leucogranites, migmatites, pegmatites, marbles and garnet-bearing schists with well-defined foliation parallel to the trend of the zone. Petrological and thermobarometric studies revealed two metamorphic stages: an early high-amphibolite facies event (Zhang et al., 1993; Heppe et al., 2007) and a later greenschist facies overprint (Zhang et al., 1993; Wang et al., 2006; Akciz et al., 2008). The early peak metamorphic conditions are equivalent to c. 30 km in depth (Meng et al., 2008). Zhang et al. (1993) suggested that the shear zone protoliths formed originally as part of an early Precambrian arc overprinted by a low-P/T regional metamorphism during the emplacement of the Lincang Granite, and that this pluton experienced a post-Triassic retrograde metamorphism (Heppe et al., 2007). During the Cenozoic the shear zone formed and exhumation (from a depth of approximately 20 km) occurred from the late Eocene to Miocene (Akciz et al., 2008).

The Ailao Shan-Red River shear zone is a major shear that separates the Yangtze blocks from Indochina (Fig. 1; Tapponnier et al., 1990; Zhong and Tapponnier, 1990; Leloup et al., 1995; Zhang et al., 2006). The shear zone exposes large-scale, high-temperature strike-slip deformation features within middle and lower crustal rocks and extends nearly 1000 km offshore. Evidence for strike-slip motion on the zone has been described by Leloup et al. (1995), and reviewed and updated by Leloup et al. (2001) and Searle et al. (2007), and so it is only briefly outlined here. Structural and geochronological studies suggest two episodes of Cenozoic strike-slip shearing on this zone. An earlier phase of left-lateral slip from Late Oligocene to Miocene resulted from the extrusion southeastward of the Indochina block (Tapponnier et al., 1986; Briais et al., 1993; Leloup et al., 1995, 2001; Lacassin et al., 1997; Gilley et al., 2003). This is widely overprinted by a major phase of dextral strike-slip since c. 5 Ma (Jolivet et al., 2001; Burchfiel and Wang, 2003; Socquet and Pubellier, 2005).

The Lanping-Simao terrane forms a continental fragment derived from Indochina separated from the Yangtze block by the Ailao Shan-Red River shear zone (Fig. 1B). Most of the Lanping-Simao terrane is covered by thick clastic sequences (up to 6 km) of Jurassic to Eocene continental red-beds (BGMRYP, 1987; Chen et al., 1995; Feng et al., 2005; Metcalfe, 2006; Peng et al., 2008; Metcalfe and Sone, 2008). Paleozoic and Triassic strata are only exposed in crests of some anticlines (BGMRYP, 1987; Wang and Burchfiel, 1997). The red-beds were folded with NW–SE to NWN–SSE trending axial planes (Fig. 2), implying an NE–ENE directed shortening compatible with sinistral shear along the Ailao Shan-Red River shear zone (Leloup and Kienast, 1993; Leloup et al., 1995). Wang and Burchfiel (1997) suggested a Palaeogene age for some of the folds and thrusts in the Lanping-Simao region. Accompanying the deformation is a phase of magmatism interpreted as being synchronous with shearing along the Ailao Shan-Red River shear zone during the Tertiary (Chung et al., 1997; Wang et al., 2001; Xue et al., 2003; Dong et al., 2005). Morley (2004) documented the development of an extensive fold belt stretching from the eastern half of Thailand through to Laos into the Lanping-Simao region and showed that it was an important belt of transpressional deformation from Late Mesozoic to Palaeogene.

The Than-Thai block is bounded by the Gaoligong shear zone to the west and the Chongshan shear zone to the east (Figs. 1 and 2). The block shows a wedge geometry with its narrower part in the north linking to the eastern Himalaya Syntaxis and its wider part in the south extending into Burma and northwestern Thailand (Fig. 1; Morley, 2007). It contains a thick section of mainly pre-Mesozoic metamorphic rocks, Late Triassic granite, arc-related volcanic-sedimentary sequences and minor Cenozoic strata (Fig. 2) (Zhong, 2000). The ages of the internal structures are unclear, but folding was followed by dextral and sinistral strike-slip faulting of early and late Cenozoic age and many of the faults are presently active (Wang and Burchfiel, 1997; Akciz et al., 2008).

3. The Chongshan shear zone

The Chongshan shear zone extends hundreds of kilometers along the Biluoxueshan–Chongshan mountain in western Yunnan with a width of c. 10 km (Fig. 2). The shear zone is divided by an N-S trending fault into two belts with contrasting metamorphic facies: an eastern lower-grade schist belt and a western high-grade gneiss belt, which were thought to be a paired-metamorphic zone (Zhang et al., 1993). The high-grade gneiss belt is mainly composed of garnet-biotite-sillimanite-bearing paragneiss, orthogneiss, augen gneiss with large feldspar porphyroblasts, migmatite, leucogranitic veins and granodiorite. A mineral assemblage of sillimanite + garnet + biotite + quartz + plagioclase + muscovite indicates an amphibolite grade metamorphism. The sub-parallel low-grade schist belt comprises severely folded phyllite with local mica schists. The low-grade schist belt is separated by faults from the Lanping-Simao terrane (Fig. 2). The degree of metamorphism and the intensity of deformation decrease from west to east (Fig. 3).

3.1. Description of ductile fabrics

Most rocks of the Chongshan shear zone developed a penetrative foliation and associated mineral lineation (Fig. 4A, B), with intense ductile shear leading to the development of mylonites: quartz grain-size reduction is widespread in the matrix, together with the development of elongate asymmetric porphyroclasts of feldspar and quartz (Fig. 4C, D). Deformed leucosome veins also form part of the shear banding (Fig. 4E–G). In the high-grade gneiss belt, foliation, marked by the preferred orientation of micas and flattened quartz or feldspar ribbons, is parallel to the macroscopic compositional

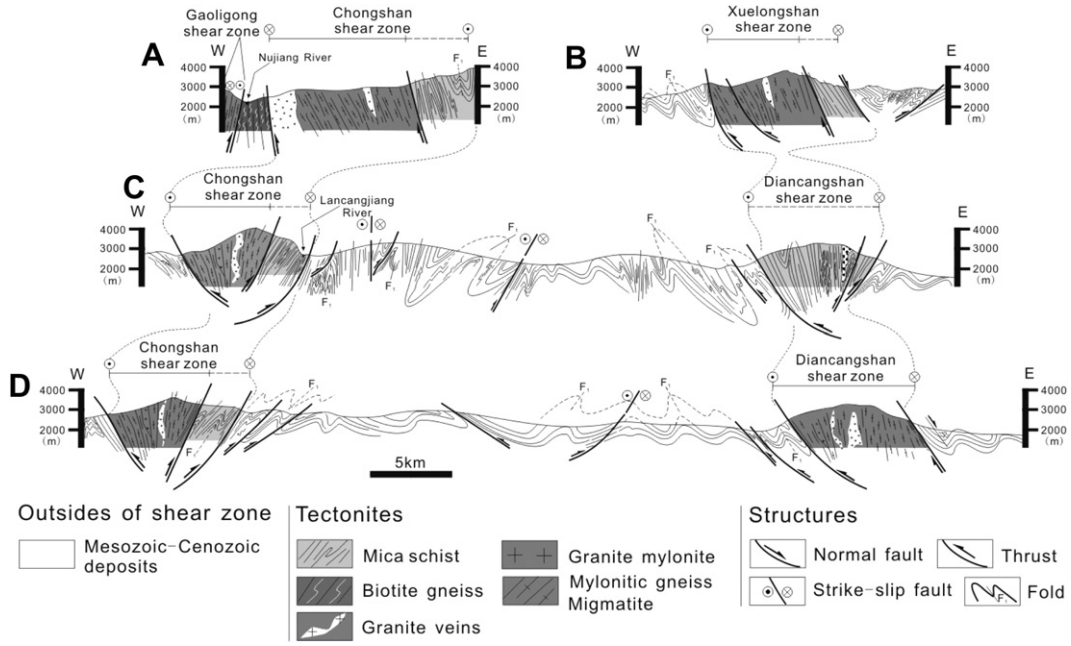

Fig. 3. Cross-sections of the Chongshan shear zone and adjacent area, including Lanping-Simao terrane and Xuelongshan shear zone and Diancangshan shear zone (location in Fig. 2).

banding. A calcite grain-shape fabric and alignment of magnesium silicates define foliations and lineations respectively in marbles. Mineral lineations in gneisses (Fig. 4A), are formed by elongated quartz and feldspar, feldspar porphyroclast tails, garnet pressure shadows and the biotite grain alignments. In the low-grade schist belt, foliation is defined by aligned biotite, muscovite and chlorite, while lineation is defined by streaking of mica domains on foliation surface (Fig. 4B). Lineation orientations across the high-grade and low-grade belts seems to be consistent in each cross-section (Fig. 2). The mineral lineation plunges northwards or southwards in the range of 0–20°, with trend of N5°E, N330°E, and S333°W, respectively, nearly parallel to the shear zone margins (Fig. 2).

3.2. Shear zone geometry

The northern Chongshan shear zone lies within and along the N–S trending Biluoxueshan mountain, where the mylonitic zone is separated by a gneiss belt along the Nujiang valley from the Gaoligong shear zone metamorphic rocks along the N–S trending Gaoligong mountain (Figs. 2 and 3A; Akciz et al., 2008). The Lishadi section, near the small village of Lishadi, preserves a well exposed section through the mylonitic rocks in the western part of the Chongshan shear zone (Fig. 3A). The section starts in the mylonitic gneiss of the Gaoligong shear zone, passes through a gneiss belt along the Nujiang River, and continues farther east into the Chongshan shear zone metamorphic rocks (Fig. 3A). The metamorphic rocks of the Gaoligong shear zone contain a steep mylonitic foliation and sub-horizontal stretching lineation with good dextral shear-sense indicators. However, the Chongshan shear zone consists mainly of mylonitic gneiss and granite, with an N–S to NNW-striking foliation and sub-horizontal stretching lineation (Fig. 2). The foliation is vertical or dips steeply to the east (Figs. 2 and 3A). The gneiss belt (Fig. 2), separating the Gaoligong shear zone from the Chongshan shear zone displays a vertical foliation without observable lineation and ductile shear-sense indicators.

In the middle Chongshan shear zone, from Fugong to eastern Liuku, the foliation geometry becomes more complex. The foliation changes from vertical in the centre to sub-vertical externally; it dips steeply to the east in the western limb, and to the west in the eastern limb (Figs. 2 and 3C, D). Most stretching lineations are sub-horizontal and plunge to the north.

In the southern segment of the Chongshan zone, near Yongping, the foliation is vertical in the centre and strikes NW–SE, but it becomes steeply westward-dipping on the eastern side, and steeply eastward-dipping on the western side, with sub-horizontal stretching lineations throughout (Fig. 2).

The strike of the sub-vertical foliation in the Chongshan shear zone varies from N–S in the north to NNW–SSE in the middle and southern segments. The geometry of the foliations in the middle and southern zone shows an “open fan” (Woodcock and Fischer, 1986) or “flower structure” geometry (Wilcox et al., 1973; Woodcock and Rickards, 2003) in vertical cross-sections (Fig. 3C, D). Stretching lineations are predominantly sub-horizontal to shallowly southward plunging in the northern segment, but become sub-horizontal to northward plunging in the middle and southern segments.

3.3. Kinematic analysis

Well-defined fabric asymmetries associated with the sub-horizontal lineation are best identified on the surfaces perpendicular to the foliation and parallel to the lineation. In the northern segment, the overwhelming majority of shear-sense indicators both in oriented thin-sections and in outcrops show dextral shear (Figs. 4C, E and 5A, B), though a small amount of sinistral shear-sense indicators are observed in some oriented thin-sections. S–C fabrics are common in fine grained granitic mylonites and leucogranite veins (Fig. 5A, B). The most spectacular examples of S–C–C′ fabrics are identified in augen gneisses from the Lishadi section, and the C′ foliation transecting the main foliation yields a dextral shear sense (Fig. 5B). The microstructures in thin sections, such as asymmetric feldspar porphyroblasts, pressure shadows and mica-fish, give kinematics consistent with the macroscopic observations, such as deformed leucogranite veins (Fig. 4E).

A sinistral shear sense for the middle and southern segments of the Chongshan shear zone is indicated by ductile deformation

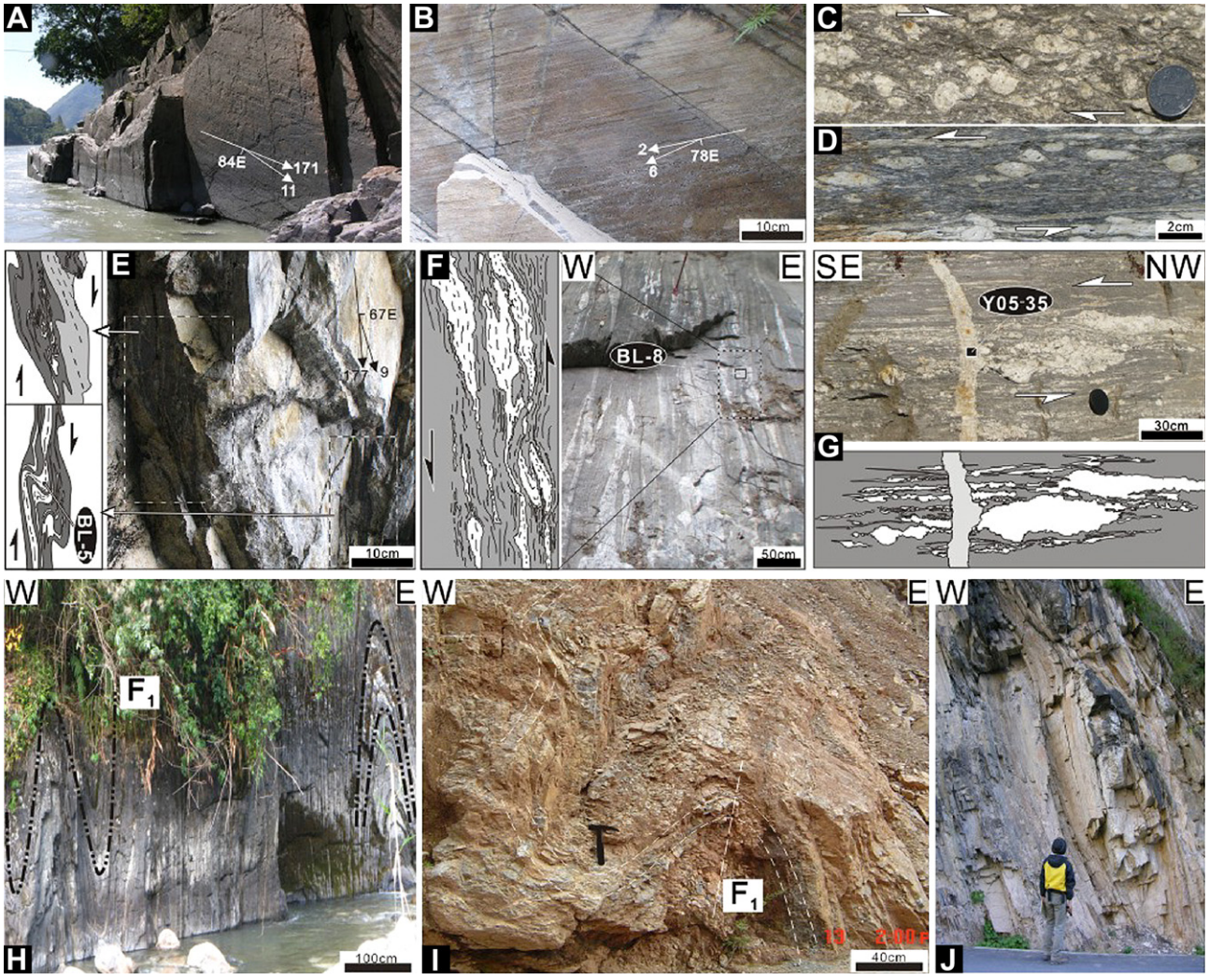

Fig. 4. Field photographs of typical structures associated with strike-slip shearing deformation found in the Chongshan shear zone and adjacent area. (A) Sub-vertical gneiss foliation with sub-horizontal mineral stretching lineation characterized by elongated feldspar and quartz crystals, indicating dextral sense of shearing, near Fugong town. (B) Nearly horizontal mineral stretching lineations on the vertical foliation of quartzite. (C) Rolling structures and asymmetric porphyroclasts in foliated granite in the northern segment of the Chongshan shear zone, northern Lishadi village. (D) Asymmetric porphyroclasts and rolling structures in foliated granitic gneiss in the southern segment of the Chongshan shear belt. (E) Folded grey gneiss and leucosome indicating dextral shearing in the northern segment of the shear zone, near Lishadi village. (F) Folded and boudinaged leucogranitic veins with sinistral shear-sense indicators, in the middle segment of the zone. (G) Undeformed leucogranite vein cutting across the earlier leucosome and foliations of the mylonitic gneiss in the southern segment of the zone. (H) Isoclinal F_1 folds in the metamorphic sandstone on the western limb of the northern Biluoxueshan, northern Lishadi village. (I) Gentle-plunging F_1 fold in the Triassic red beds, near Lanping town. (J) Large boudins in the Triassic rocks, near Lanping town. Noted that some sampling locations for U–Pb geochronology. Observable panels C–G are perpendicular to foliation and parallel to stretching lineation.

indicators in rocks. These well-developed indicators include micro-fractures (Fig. 5C, D), σ-type porphyroclasts (Figs. 4D and 5E), folded quartz veins and asymmetric mica-fish (Fig. 5F). Folded and boudinaged leucogranitic veins also show a sinistral strike-slip shear sense, similar to the host gneiss (Fig. 4F, G).

3.4. Fold

Two types of folds can be recognized in the Chongshan shear zone and the adjacent regions, both in the field and on the equal-area plots (Figs. 4H, I and 6A). The major type is larger F_1 folds. The other type is marked by smaller F_2 folds. In most outcrops, F_2 folds are observed superposed on the limbs of the larger F_1 folds. The F_1 folds have sub-horizontal hinges while the F_2 folds are steeply plunging to sub-vertical (Fig. 6A). F_1 folds were observed in all stratigraphic units east of the Chongshan shear zone, but these folds do not develop to the same deformation intensity. F_1 folds are common in early Jurassic, Cretaceous, Paleocene–Oligocene strata where they developed upright horizontal to inclined horizontal axial planes, while those near the Ailao Shan-Red River shear zone trend NW–SE and verge SW (Fig. 3B, C, D). F_1 folds in the schist of the Chongshan shear zone are generally asymmetric with east-dipping axial planes with gently N–S plunging hinges (Figs. 3 and 6A). Layers are thickened in the hinges and thinned on the limbs and boudins of Triassic marble on the limbs are observed (Fig. 4J). Trends of F_1 folds in the central area of the Lanping-Simao terrane are slightly oblique (less than 10°) to the two boundary shear zones, but they curve into the shear zones as approaching the latter (Figs. 2 and 6D).

Macroscopic F_2 folds are mainly identified in the metamorphic zone and limbs of F_1 folds in the red-beds of the Lanping-Simao terrane (Fig. 6A–C). These F_2 folds of S_0/S_1 compositional layering plunge steeply with high dipping, nearly NNE–SSW trending axial planes in the red-beds (Fig. 6A). F_2 folds are common in the leucogranite intruding the high-grade gneiss belt, in which they are characterized by locally rootless and highly boudinaged limbs (Fig.

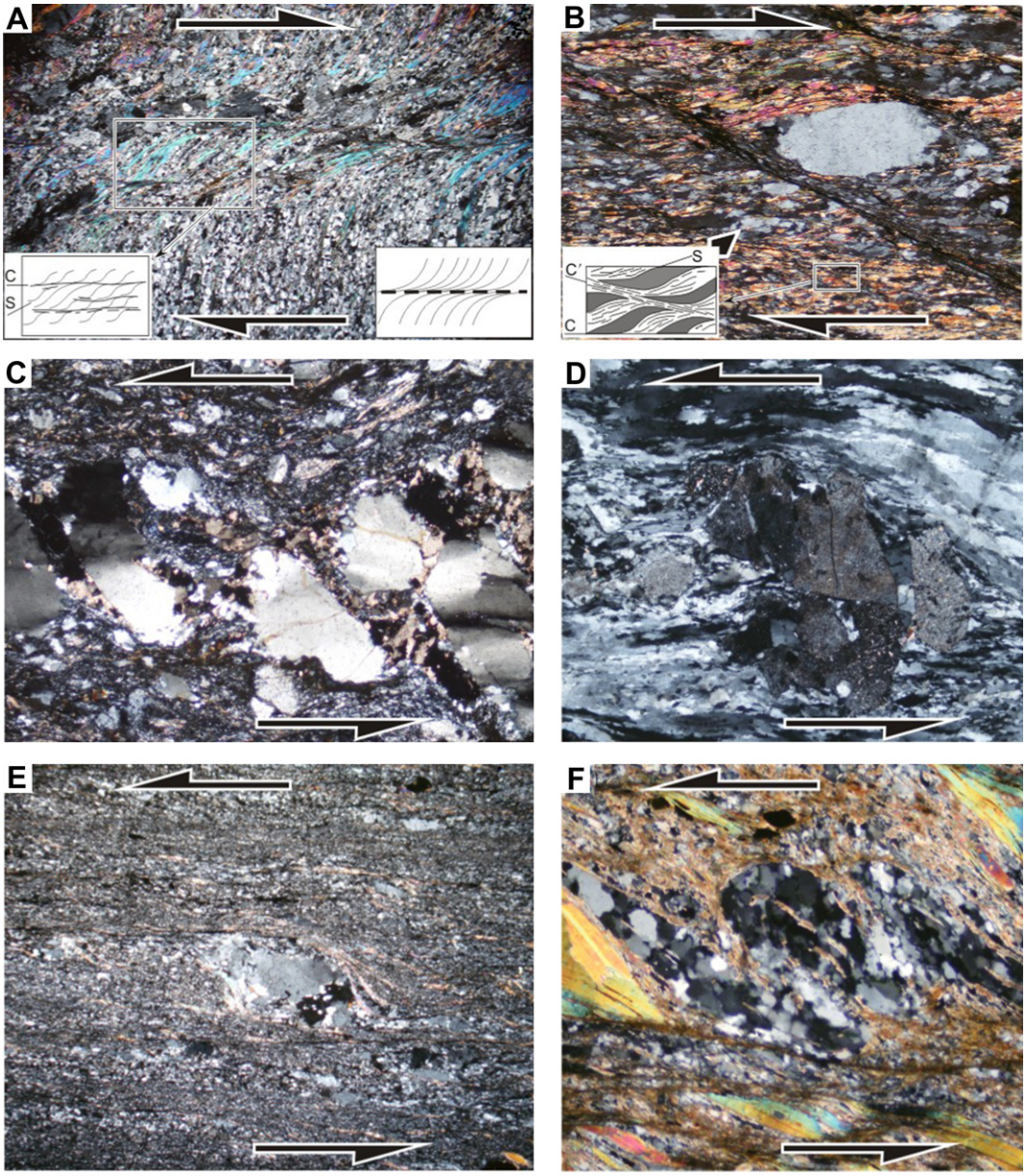

Fig. 5. Microstructures of typical examples in mylonites from the Chongshan shear zone. All thin sections parallel to the stretching lineation and normal to the foliation. Width of view 5 mm for A, B, E, and F; 1 mm for C and D. Crossed polarized light. (A) Foliation deflection and S–C fabric in the quartz–feldspar–muscovite mylonite BL-5. C-planes are horizontal, S-planes trend upper right to lower left between C-Planes. Dextral shear sense. (B) C′-type shear zones with S–C fabric in the quartz–feldspar–mica mylonite BL-9. Dextral shear sense. (C) Quartz porphyroclast with undulose extinction and micro-fracture. Mantles of recrystallized quartz and mica surround the porphyroclasts. Sinistral shear sense. Mica-bearing mylonite BL-34. (D) Boudinaged feldspar fragments separated by quart-filled transverse vein. The micro-fractures do not continue into the mantle of recrystallized quartz surrounding the porphyroclasts. Notice the strongly elongated polycrystalline quartz ribbons. Sinistral shear sense. Muscovite-bearing granitoid mylonite Y05-21. (E) A sigma-type feldspar porphyroclast surrounded by dynamically recrystallized quartz and feldspar. Sinistral shear sense. Mica-bearing mylonite BL-42. (F) A folded quartz vein in the micaschist of the southern segment of the zone, near Yongping region. Sinistral shear sense.

4E, F). The asymmetry of F_2 folds shows similar shear-senses to nearby ductile shear sense indicators (Fig. 4F).

3.5. Cleavage

A strong slaty cleavage (S_1) is developed in the folded schist and younger folded red-beds lying parallel to the axial planes of F_1 folds (Fig. 6B), with an N–S or NNW–SSE trend. Intersections of S_1 and the bedding (S_0) plunge shallowly to N or S (Fig. 6C). Some late cleavages are developed locally in the mica-schist of the Chongshan zone and in the most tight-upright F_1 folds of Jurassic and Cretaceous rocks beyond the metamorphic zone. These crenulation cleavages trend NW–SE and E–W respectively, and cut S_1 cleavages at a high angle.

3.6. Conjugate sets of strike-slip faults

A network of conjugate brittle strike-slip faults is exposed within the study region, especially in the low-grade schist belt and the Lanping-Simao terrane, which provide the best opportunity to study the brittle structural geometries and linkages to the ductile deformation on the larger scale.

These sub-vertical strike-slip faults are identified in the field and map-scale, based on the 1:200,000 geological maps (BGMRYP, 1987; Figs. 6D and 7). One set shows right-lateral slip and the other left-lateral slip (Fig. 6D and E). As illustrated in Fig. 6D, dextral faults are more common than sinistral ones. The mean trend of sinistral faults is about 090°–110°, whereas dextral faults

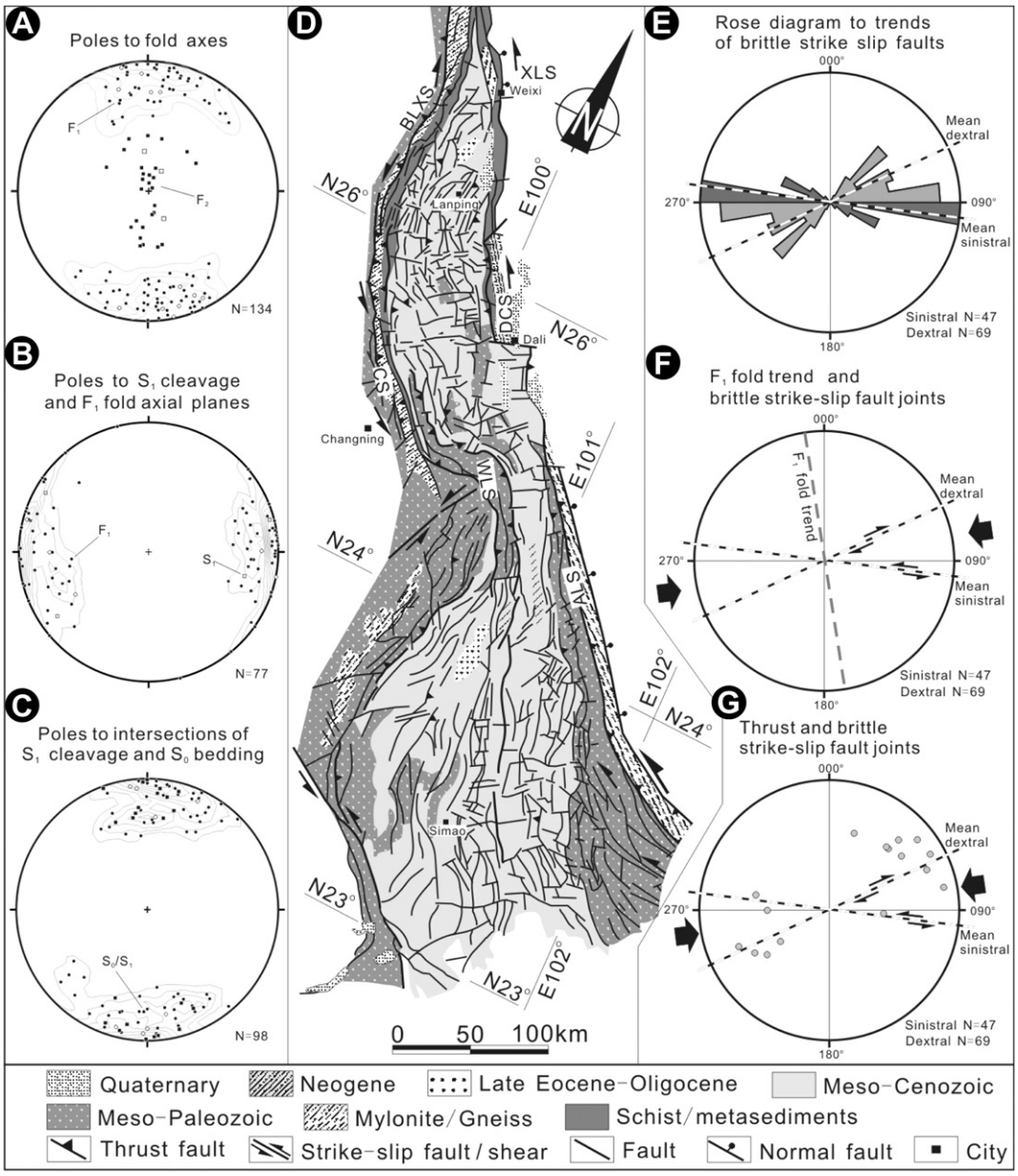

Fig. 6. Stereograms of the structural elements within the Chongshan shear zone and the Lanping-Simao terrane. Equal-area projection, lower hemisphere. (A) F_1 and F_2 fold axes. Solid dots denote F_1 fold axes in Mesozoic strata. Open circles represent F_1 fold axes in Cenozoic strata. Solid squares represent F_2 fold axes in Mesozoic strata, schist and shear zones. Open squares represent F_2 fold axes in Cenozoic strata. (B) F_1 fold axial surface (Solid dots for Mesozoic strata, open circles for Cenozoic strata) and S_1 cleavage (Solid squares for Mesozoic strata, open squares for Cenozoic strata). S_1 cleavage is parallel to F_1 fold axial surface. (C) Poles to S_0/S_1 intersectional lineations. (D) The structural elements in the Lanping-Simao terrane and its two boundary shear zones, the Chongshan and Ailao Shan-Red River shear zones. (E) Rose diagrams of the trends of brittle strike-slip faults. (F) Equal-area plot (lower hemisphere) of strike-slip faults on one outcrop of the basin, indicating a nearly E–W contraction sub-normal to the average F_1 fold trend. (G) Equal-area plot (lower hemisphere) of strike-slip faults and thrust faults (grey circles) in the region, indicating ENE–WSW-shortening sub-normal to the thrust faults. Abbreviations: BLXS, Biluoxueshan; CS, Chongshan; WLS, Wuliangshan; XLS, Xuelongshan; DCS, Diancangshan; ALS, Ailaoshan. Data (E, F and G) measured in the field and on 1:200,000 geological maps (BGMRYP, 1987, 1990).

trend 070°–090° (Fig. 6E). The two sets of faults are conjugate about an approximately E–W horizontal shortening axis consistent with the nearly N–S trending F_1 folds and thrusts (Fig. 6F, G) and the foliations of the mylonites within the Chongshan shear zone (Fig. 6D).

4. Generations of structures

Three generations of structures are recognized within the Chongshan shear zone and adjacent regions. N–S to NNW–SSE trending F_1 folds with axial planar cleavage S_1 are deduced to be the earliest structures (D1). D1 features are observed in the low-grade schist belt and adjacent strata of the Lanping-Simao terrane.

The D2 structures comprise sinistral ductile shear, the development of boudinage and F_2 folds within the studied regions. They formed after F_1 folds and caused the local refolding and transposition of S_1.

Brittle fractures, including the conjugate strike-slip faults formed the third generation of structure (D3). The traces of D3 structures cut those of D1 and D2 features. The faults displaced F_1 folds, slaty cleavages and foliations of mylonites.

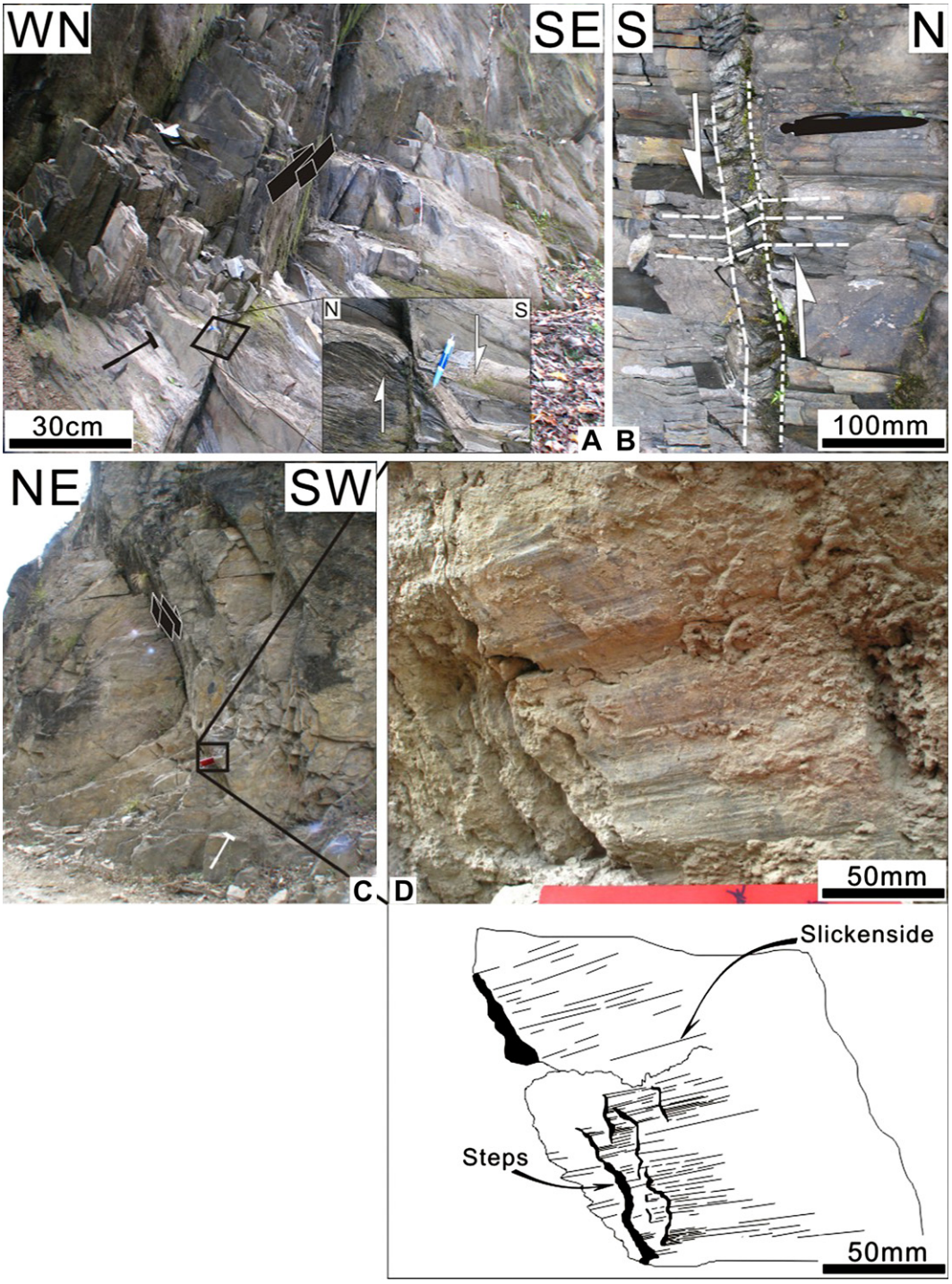

Fig. 7. Strike-slip faults and fractures within the Chongshan shear zone and adjacent area. (A) ENE–WSW trending dextral strike-slip fault in metasandstone. (B) Kink-band with sinistral sense. (C) ESE–WNW trending dextral strike-slip fault in Cenozoic sandstone strata; (D) Steps and sub-horizontal slickensides on the fault surface.

5. U/Pb geochronology

We present new U–Pb isotopic data from LA-ICPMS and SHRIMP analyses that provide age constraints for magmatism, metamorphism and deformation associated with the development of the Chongshan shear zone. Sample locations are given in Fig. 2. The U–Pb analytical procedure and all analytical data are provided as an electronic supplement (Appendices A and B).

5.1. Sample relationships to Chongshan shear zone deformation

Sampling for this work focused on samples that can place better age constrains on the early magmatic and metamorphic evolution, and subsequent strike-slip deformation within the Chongshan shear zone. The mylonitic gneisses are associated with a number of leucogranite veins. The belts crossing granitic veins are parallel or cross-cut at low angles relative to the foliation in the host mylonitic

gneisses. A few veins completely transect a mylonitic fabric, but most are weakly or strongly deformed within the mylonitic gneiss and show similar deformation structures (Fig. 4E–G).

Ten samples were taken from the Chongshan shear zone (Fig. 2). Four samples (BL-1, BL-2, BL-3, BL-5) were from the northern segment of the shear zone, three samples (BL-8, BL-12, BL-13) from the middle segment, and other three (Y05-30, Y05-35, Y05-39) from the southern segment of the zone.

5.2. Zircon morphology and U–Pb ages

5.2.1. BL-1: intensely deformed paragneiss

Sample BL-1 is a banded migmatitic paragneiss with a mylonitic fabric. It contains the mineral assemblage sillimanite–garnet–biotite–K-feldspar–plagioclase–quartz–graphite, which indicates peak high-amphibolite facies metamorphic conditions (BGMRYP, 1987; Akciz et al., 2008). CL images of zircon crystals both small and large, contain a well-defined core, surrounded by rather wide rims that typically show euhedral, oscillatory zoning (Fig. 8, grain A, B). The shapes of the cores vary from irregular (Fig. 8, grain B), angular to rounded and in some cases they are roughly euhedral (Fig. 8, grain A). The zoning pattern in the rim is discordant to zoning of the cores. On irregular cores, the rim growth starts by filling out the irregularities before building the euhedral oscillatory zones (Fig. 8, grain B).

Nineteen zircon analyses, located on the tips, were given by LA-ICPMS. The data show two distinct age populations and show strongly scatter, one at c. 84–55 Ma and the other at c. 188–128 Ma (Fig. 9A). U and Th contents are variable resulting in very variable Th/U values, e.g. 0.05–0.11 for the population < 100 Ma, 0.14–0.45 for the population > 100 Ma. This suggests growth in a chemically heterogeneous environment (Zeck et al., 2004), with lower Th/U values for younger zircons indicating a metamorphic trend (Zeck and William, 2002; Zeck and Whitehouse, 2002). All analyses are slightly normally discordant (Fig. 9A). A regression line through almost all data points (15 of the 19 data) yields a lower intercept age (Ludwig, 2003) of 24.7 ± 9.8 Ma (MSWD $= 1.8$), which is our best estimate for the timing of metamorphism affecting this rock, and an upper intercept age of 619 ± 50 Ma. The normal discordance of all data points indicates that there is a component of inheritance. Because all data are scattered, the calculated upper intercept, 619 ± 50 Ma likely reflects a real thermal event in which new zircon growth has occurred.

5.2.2. BL-2: deformed gneiss

Sample BL-2 is from the foliated and weakly banded quartz + plagioclase + orthoclase + biotite gneiss. The zircons are commonly elongated, with euhedral prisms up to 200 μm. Optical and by CL imaging shows that the prismatic grains display a strong micro-scale oscillatory zoning typical of magmatic zircons (Fig. 8, grain C, D). A minority of zircon grains contain cores of rounded or irregularly shaped older zircons (e.g. Fig. 8, grain C).

Altogether, seven U–Pb SHRIMP spot analyses have been made on six zircons. Common Pb is typically low ($<0.8\%$ of ^{206}Pb), although it is as high as 1.3% in one analyses (BL-2-5.1). Th/U ratios typically range between 0.18 and 0.48, inferring a magmatic origin. Two analyses from xenocrystic zircon grains (BL-2-8.1 and BL-2-1.3) show inheritance ages at 1203 and 581 Ma. Five analyses obtained in oscillatory zoned zircon form a distinct cluster (Fig. 9B). The analyses are entirely concordant, and one analysis is significantly older than the rest. All in all the four analyses reveal a $^{206}Pb/^{238}U$–$^{207}Pb/^{235}U$ concordia age of 213 ± 5.5 Ma, MSWD $= 1.4$ (Fig. 9B), which is to interpret as the magmatic age of the orthogneiss protolith.

5.2.3. BL-3: granitic pegmatite boudin

Sample BL-3 is a boudinaged granite pegmatite vein, preserved within augen gneisses from the Chongshan shear zone close to BL-5. The pegmatite is locally retrogressed, with biotite replaced by medium-grained chlorite. The morphology of Zircon grains is commonly euhedral, up to 250 μm. Zircon grains are characterized by moderately to highly luminescence with variable internal zoning patterns, such as oscillatory zoning (e.g. Fig. 8, grain E, F). Patchy zoned domains (e.g. Fig. 9, grain F) are characterized by weakly or moderately luminescent zircons that may form rims on the oscillatory zoned luminescent zircons. These rims are typically euhedral, but show localized rounding of terminations.

Nine spots placed in oscillatory zoned rims, yielded two distinct concentrations. One along or near the concordia curve gave ages around 45 Ma whilst the other yielded ages of about 49 Ma (Fig. 9C).

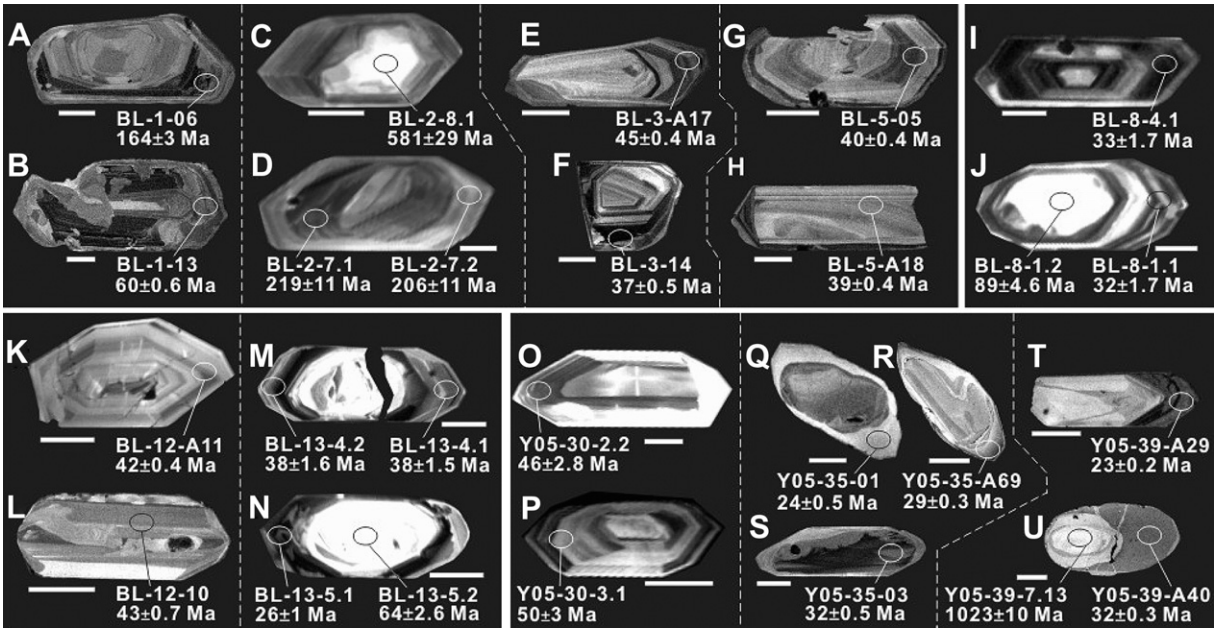

Fig. 8. SEM images of representative zircons with analytical spots and their resulting ages from the Chongshan shear zone. Scale bars all represent 100 μm. See Appendices A and B for analytical data by LA-ICPMS and SHRIMP, respectively.

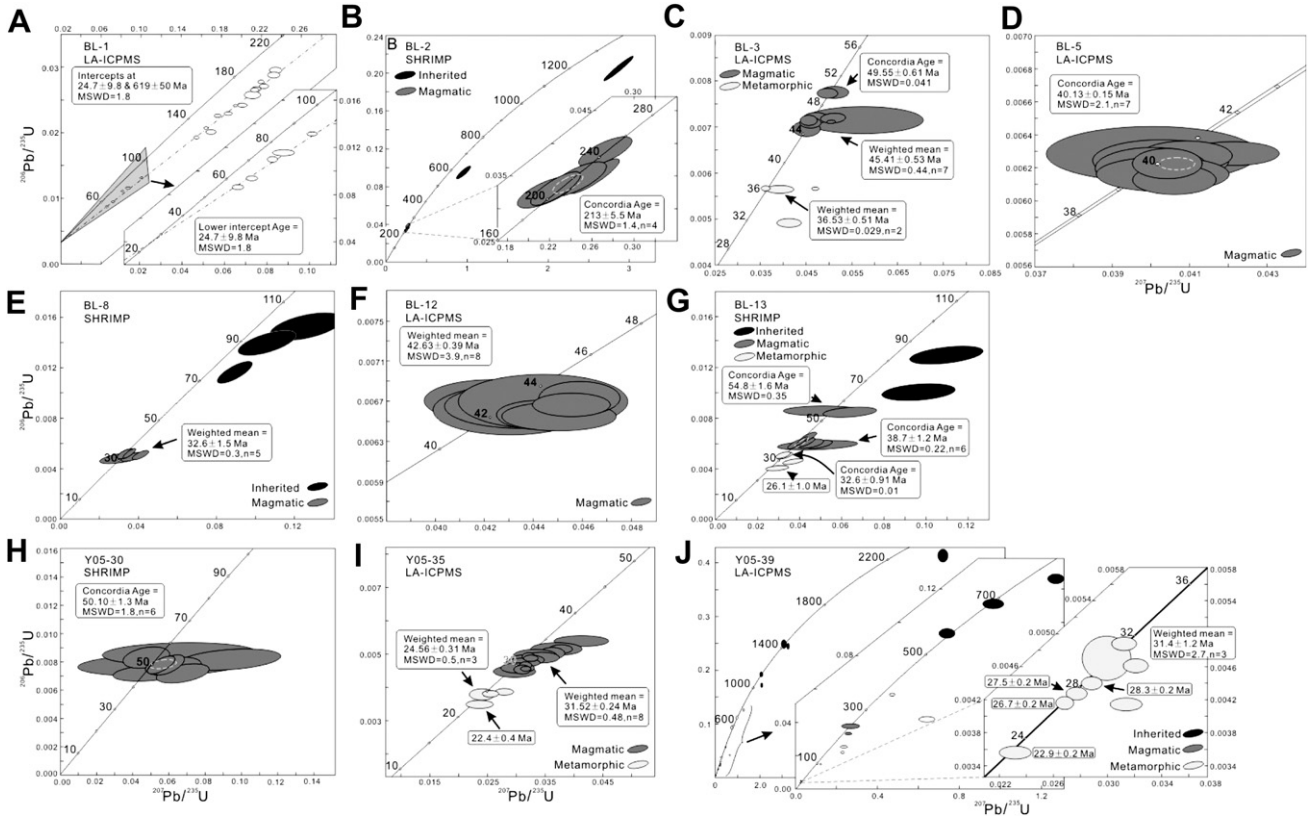

Fig. 9. Wetherill concordia plots of LA-ICPMS and SHRIMP U-Pb zircon data from the granitic veins and gneisses in the Chongshan shear zone.

Two data on the concordia curve and reveals a concordia age of 49.55 ± 0.61 Ma (MSWD = 0.04). The oscillatory zoned nature of all seven dissected zircon rims indicates a melt crystallization. Therefore, the mean age (45.4 ± 0.53 Ma) as well as the concordia age (49.55 ± 0.61 Ma) are interpreted as the crystallization age of the granitic pegmatite vein. A further analysis has been done in four patchy zoned rims (e.g., BL-3-14), which are characterized by generally low Th contents (114-43 ppm) and the lowest Th/U ratios (between 0.06 and 0.11); this yields a mean Eocene age of 36.53 ± 0.51 Ma ($n = 2$, MSWD = 0.03). Two other analyses are significantly more discordant. These Latest Eocene ages (36.53 Ma) probably represent zircon recrystallization during a high-grade metamorphic event. Hence, we interpret the 49.55 ± 0.61 Ma and 45.4 ± 0.53 Ma ages to reflect the intrusion age of the granitic pegmatite vein, and 36.53 ± 0.51 Ma to record the timing of subsequent metamorphism.

5.2.4. BL-5: folded leucosome

Sample BL-5 is a medium-grained muscovite-biotite-quartz-plagioclase-bearing leucosome within sillimanite-biotite-garnet-muscovite mylonitic gneiss. The leucosome is concordant with the sub-vertical foliation of the gneiss. Both the leucosome and gneiss foliation have been folded by dextrally verging (F_2) folds, consistent dextral strike-slip shearing (Figs. 2 and 4E). Similar leucosome nearby is boudinaged and folded, and indicates an extension direction consistent with the regional stretching direction. Zircon grains are euhedral and colourless to light brown in transmitted light, with oscillatory zoning evident in CL images (Fig. 8, grains G, H). Most grains have length/width ratios of about 3:1, and lengths of about 250 μm.

Eight analyses of zircons have been made by LA-ICPMS, focusing on igneous morphologies. Analyses of zircon grains have higher Th/U ratios between 0.10 and 0.42, with two analyses relatively low (c. 0.03), with moderate to high concentrations of U (831–4550 ppm). The majority of the analytical population is concordant (Fig. 9D), producing a concordia age of 40.13 ± 0.15 Ma ($n = 7$, 95% confidence limit; MSWD = 2.1), interpreted to be the crystallization age for the rock.

5.2.5. BL-8: deformed granitic vein

Sample BL-8 comes from a deformed granitic vein in the middle segment of the Chongshan shear zone (Fig. 2). Some of the leucogranite veins occurred in layers parallel to the shear-induced planar foliations in the host gneisses (Fig. 4F). These veins show weak foliation and lineation indicating that crystallization locally occurred concurrently with late phases of sinistral lateral shear. However, other veins cross-cut the mylonitic fabrics of the host at low angles (Fig. 4F), show boudinage and display mylonitically fabrics in thin section. Zircon grains occur as elongate, stubby, subhedral to euhedral forms, most preserving similar internal zoning characteristics (Fig. 8, grain I). A few grains include rounded, moderate to strongly luminescent cores, which show weak patchy zoning patterns truncated by oscillatory zoned mantles (Fig. 8, grain J). These inner cores are interpreted to be inherited. Moderate to weakly luminescent oscillatory zoned grains form the dominant population, and occur as both cores and as mantles to inherited grains. Oscillatory zoning is typically parallel to the external crystal faces of euhedral grains (e.g. Fig. 8, grain I).

SHRIMP analyses of the prismatic, euhedral zircon tips show high U contents (all > 1000 ppm) and high Th/U (>0.1), with one analysis having a low Th/U (BL-8-4.1, 0.04). Pooled together, the data yield a weighted mean $^{206}Pb/^{238}U$ date of 32.6 ± 1.5 Ma (MSWD = 0.30) (Fig. 9E). Given the character of these zircons, and the field and petrographic observations, it is suggested that these

represent the igneous ages of the syn-shearing veins. Three structural cores detected by CL imaging yield older dates; 88.8 ± 4.6 Ma (1σ, site BL-8-1.2), 74.5 ± 3.9 Ma (1σ, site BL-8-9.1) and 97.7 ± 5.1 Ma (1σ, site BL-8-11.1), which all lie slightly below the concordia. The older ages are indicative of inclusion of inherited older crustal material in the acidic magma.

5.2.6. BL-12: deformed leucogranite vein

Sample BL-12 is from a medium-grained leucogranite vein that is folded by F_2 as well as boudinaged. The near-vertical axial planes of the F_2 folds are concordant with the transposition foliations in the host gneiss, and the F_2 folds indicate sinistral strike-slip motion. The vein has a foliation defined by flattened feldspar, quartz and mica, which is parallel to that of the host gneiss, but the stretching lineation is weak. Most of the zircon grains from leucogranite BL-12 are euhedral and show oscillatory zones of typical igneous zircons (e.g., Fig. 8, grains K, L). They have length/width ratios of ~3:1 and lengths of ~200 μm.

A total of eight analyses made by LA-ICPMS in either oscillatory zoned and planar banded mantles or rims form a single group. Five zircon analytical U–Pb data lie on a concordia; other three analyses lie slightly below the concordia (Fig. 9F). These concordant and discordant data appear typically tight and partly overlapped each other, producing a weighted mean age of 42.63 ± 0.39 Ma ($n = 8$, MSWD = 3.9). This is interpreted to be the igneous age.

5.2.7. BL-13: weakly deformed granite

Sample BL-13 is a weakly deformed, medium-grained granite, located close to the sampling site of sample BL-12 (Fig. 2). The granite shows a weak foliation defined by trails of muscovite, biotite, locally retrogressed to chlorite. The zircon grains separated are mostly 200–250 μm prismatic crystals or crystal fragments. In most prismatic crystals, micron-scale oscillatory zoning is evident and the features are those of a simple, magmatic population (Fig. 8, grain M). These zircon grains include rounded, strongly luminescent cores, which show patchy banding patterns truncated by oscillatory zoned mantles (e.g., Fig. 8, grain M), and may be locally truncated and embayed along curved fronts by younger rims (Fig. 8, grain N). These rims are typically thin, weakly luminescent, and exhibit patchy banding.

Sample BL-13 was analyzed by SHRIMP. Using CL imagery, possible inherited cores are present in a few grains. Two cores were analyzed, which yielded a Late Cretaceous $^{206}Pb/^{238}U$ age of 83.1 ± 3.3 Ma and a Earliest Paleocene $^{206}Pb/^{238}U$ age of 64.2 ± 2.6 Ma (Fig. 9G). The core zircons from BL-8 also preserve Late Cretaceous $^{206}Pb/^{238}U$ ages of 88.8 ± 4.6, 74.5 ± 3.9, and 97.7 ± 5.1 Ma and lie slightly below the concordia curve (Fig. 9E), suggesting that it is discordant due to partially lost Pb. These cores are interpreted as xenocrysts. Analyses of the oscillatory zoned rims surrounding these cores, which we interpret as magmatically crystallized zircon, form two populations characterized by higher Th contents (>100 ppm) and somewhat higher Th/U (> 0.1, except BL-13-2.1 with Th/U = 0.04). They form two concordant groups with a concordia age of 54.8 ± 1.6 Ma ($n = 2$, MSWD = 0.35), and a lightly younger concordia age of 38.7 ± 1.2 Ma ($n = 6$, MSWD = 0.22). The two concordia ages of the zircon rims in sample BL-13 are considered to be the best estimate of the time of magmatic crystallization. The younger concordia age of 38.7 ± 1.2 Ma is similar to the age of zircons analyzed in Sample BL-5 located elsewhere in the Lishadi, northern segment of the zone. Although many zircon crystals show thin, dark CL outer rims (e.g. Fig. 8, grain N), only four crystals have rims sufficiently wide and free of inclusions, cracks and holes to allow analysis. The discontinuous, very dark CL rims of the crystals are over 30 μm wide and show irregular patchy zoning (e.g. Fig. 8, grain N). Two analyses were obtained (spots BL-13-1.1, 3.1) yielding a concordia age of 32.6 ± 0.91 Ma (MSWD = 0.01); the remaining two rim analyses (spots BL-13-5.1, 6.2) produced ages of 29.7 ± 1.2 Ma slightly below the concordia curve, and 26.1 ± 1.0 Ma on the concordia. These thin overgrowths of lowest Th content (43–90 ppm) and Th/U ratio (c. 0.02) are possible evidence to suggest an Oligocene overprint, which resulted from a thermal disturbance in two or three younger events or during a continuing younger event, possibly at 32.6 ± 0.91 Ma, c. 29.7 ± 1.2 Ma, and as late as c. 26.1 ± 1.0 Ma.

5.2.8. Y05-30: granitic pegmatite boudin

Sample Y05-30 comes from a deformed and boudinaged granitic pegmatite vein that lies parallel to the foliation in an intermediate-mafic orthogneiss of the southern segment of the Chongshan shear zone, near Yongping. The pegmatite is composed of a coarse-grained quartz-K-feldspar-plagioclase assemblage with minor chlorite. The vein is boudinaged, with the inferred direction of stretching oriented nearly N–S, sub-parallel to the foliation in the orthogneiss. The Zircon grains chosen are prismatic and euhedral, between 150 to 350 μm in length (e.g., Fig. 8, grains O, P). The colour varies from pink to light brown. CL images reveal that many zircons include subhedral to euhedral cores, in weakly to moderately luminescent grains, that are easily distinguished from rims and mantles (e.g. Fig. 8, grains O, P). These mantles and rims range in thickness from a few microns to >50 μm, and are more extensively developed on grain terminations. They typically preserve well-defined oscillatory zoning of probable magmatic origin (Fig. 8, left rim grain P).

Nine analyses made by SHRIMP, yielded one broad age cluster between 45 and 55 Ma near the concordia curve that directly relate to the zircon morphology (Fig. 9H). The nine data come from weakly luminescent grains, with locations chosen to analyze oscillatory zoned mantles and rims. These data have high Th/U ratios (0.1–0.7), and high U concentrations (280–6927 ppm). The concordia age of 50.1 ± 1.3 Ma for six zircons (MSWD = 1.8) should represent the age of pegmatite crystallization.

5.2.9. Y05-35: undeformed leucogranite vein

Sample Y05-35 comes from an undeformed, crosscutting leucogranitic vein (Fig. 4G). Foliation within the host gneisses is truncated by the strongly discordant margins of the vein. In thin section, randomly oriented, euhedral or subhedral minerals with uniform extinction indicate little or no strain. The rock is locally retrogressed, with biotite replaced by fine-grained chlorite. Based on internal zoning patterns of zircons, two populations have been distinguished. Population one zircon occurs with rounded and reabsorbed inner cores that show weakly or moderately luminescence. These are typically stubby to moderately elongate in shape (e.g. Fig. 8, grains Q, R, S). Population two zircon, which commonly forms mantles or rims, can be homogenous (e.g. Fig. 8, grain Q), weakly zoned, planar banded (e.g. Fig. 8, grains R, S), or sector zoned. Planar banded and sector zoned zircons in this sample can indicate one or more episodes of zircon growth (Vavra et al., 1996, 1999).

In total, 19 analyses have been made by LA-ICPMS. Two distinct rim types can be recognized. The first type is characterized by generally high Th content (288–1882 ppm) and high Th/U ratios (>0.1) and gives a weighted mean Early Oligocene age of 31.5 ± 0.24 Ma ($n = 8$, MSWD = 0.48) after eliminating seven analyses on the basis of excess scatter (Fig. 9I). This Oligocene group has a similar mean age as that recorded by geochemically similar zircons in BL-8. It is interpreted as dating magmatic zircon growth during the same magmatic event. The second rim type is characterized by patchy and unzoned overgrowths on the tips of grains, and low Th (65–412 ppm) and low Th/U ratios (<0.1). Four analyses

from this rims form a broad cluster at c. 24 Ma with scatter along the concordia curve to give a younger age of 22.4 ± 0.4 Ma (Fig. 9I). Their low Th contents and correspondingly low Th/U ratios are typical of metamorphically recrystallized zircon (Vavra et al., 1996; Hoskin and Black, 2000). Therefore, it is possible that the outer rims and tips reflect a younger metamorphic event during Latest Oligocene to Early Miocene high-grade metamorphism. The scatter along the concordia of data from the magmatic and metamorphic zircons may result from this overprinting event.

5.2.10. Y05-39: migmatitic gneiss

Sample Y05-39 is a coarse grained, well-foliated migmatitic gneiss, which includes rolled-garnets set in a groundmass of biotite, muscovite, quartz and feldspar. The zircon grains from sample Y05-39 preserve some prism faces (e.g., Fig. 8, grain T), but have rounded terminations (e.g., Fig. 8, grain U). Many crystals exhibit domains of dark and homogeneous CL zircon replacing oscillatory zoned zircon (e.g., Fig. 8, grain T), or overgrowing strongly-luminescent cores (e.g. Fig. 8, grain U). This type of dark CL zircon does not show rims, but occupies crystal tips and other irregular domains. Most zircon grains with rounded terminations have rounded inner cores, which show strong luminescence, and are interpreted to be inherited xenocrysts (e.g. Fig. 8, grain U).

Analyses were carried out using LA-ICPMS. The nine inherited cores identified in the zircons yielded Precambrian ages, ranging from c. 2225–576 Ma (Fig. 9J). Two zircon cores yielded Triassic $^{206}Pb/^{238}U$ ages at 233 ± 4 and 211 ± 2 Ma. In addition, five zircon cores yielded a Late Cretaceous to Early Carboniferous age range, which are highly discordant and do not necessarily indicate zircon formation at that time. It is more likely that these zircons formed earlier and lost Pb during the Tertiary to produce these mixed ages (Ring and Collins, 2005). These cores are considered to represent the zircon inherited from the rocks that contributed to the granitic melt. Eight analyses were made in dark and grey CL zircons (e.g., Y05-39-A29, Y05-39-A40). The U content in this type of zircons is high (2234–15,302 ppm) and Th content low (25–351 ppm) resulting in very low Th/U values (0.005–0.08). These data scatter between 31.3 ± 0.2 and 22.9 ± 0.2 Ma along the concordia curve (six analyses), with two analyses slightly below the Concordia. These younger ages come from overgrowths on the tips of grains, which possibly reflect one or more younger metamorphic events, during the Oligocene from 31.4 ± 1.2 to 22.9 ± 0.3 Ma. This Oligocene group has similar ages to those recorded by geochemically similar zircons in BL-13 and BL-35, and thus probably represent zircon recrystallization during the same metamorphic event.

5.3. Analysis and interpretation of the U–Pb ages

Interpretation of the U–Pb SHRIMP and LA-ICPMS ages hinges on the internal structures recognized in the analyzed zircons and the structural features observed in the outcrops and thin sections (Zeck et al., 2004). Based on this information we can recognize and date several stages of zircon generation during Cenozoic. Probability density curves and histograms for the various age clusters are shown in Fig. 10A.

5.3.1. Inherited zircon

Texturally discordant zircon cores have outlines and internal zoning patterns that are truncated by the zoning in the surrounding 213 ± 5.5 Ma magmatic (BL-2) and c. 32–22 Ma metamorphic (Y05-39) zircons, suggesting that these cores are exotic. This is confirmed by their typically older, c. 2200–500 Ma ages. It is therefore concluded that these cores are inherited from a Precambrian source.

The presence of inherited zircons in gneisses BL-2 and Y05-39 indicates that a part of the melt or all melts were derived from ancient material. Taken together with the upper intercept age from sample BL-1, the results suggest that the relicts of Precambrian crustal material are preserved in the high-grade metamorphic rocks of the Chongshan shear zone.

5.3.2. Triassic granite intrusion (c. 213 Ma)

The Triassic ages (e.g. 213 ± 5.5, 211 ± 2, and 233 ± 4 Ma) proposed here for the intrusion age of the Chongshan orthogneiss protolith are similar to the dominant regional magmatism, such as the Lincang Granite (Fig. 1) (Chen, 1987; Liu et al., 1989; Zhong, 2000). The age of the Lincang granite is considered to extend from the Permian to the Triassic, with whole-rock Rb–Sr ages documented by Chen (1987) having a peak range of 297–279 Ma, but showing a considerable total spread between 348 and 236 Ma. U–Pb ages from zircons have yielded Triassic magmatic ages between 254 and 212 Ma (Liu et al., 1989). A Triassic age of intrusion is further supported by U–Pb SHRIMP studies (Heppe et al., 2007). Further south, in northern Thailand (Chonglakmani et al., 2001), granitoid intrusions belonging to the northern Thailand Granite Complex show Triassic ages (Cobbing et al., 1986; Searle et al., 2007). Both the Lincang Granite and northern Thailand Granite Complex are thought to have been exhumed following strong Indosinian orogenesis at the end of the Triassic and that they represent the former root zone of an island arc (Heppe et al., 2007).

5.3.3. Eocene intrusion ages of granitic magma (c. 55–38 Ma)

Oscillatory zoned zircons from five deformed granitic samples yield ages that are interpreted as the best estimate for the age of the main magmatic zircon crystallization. This supports the existence of an Eocene phase of granite intrusion that lasted at least from 55 to 38 Ma (Fig. 10B). Five small peaks in the broad probability diagram imply more than one age event (Fig. 10B). For example, the age of sample BL-3 (45.41 ± 0.53) corresponds to a U–Pb age of 46.3 ± 0.6 Ma for a granite vein from the Mogok metamorphic zone, western Shan-Thai block (Searle et al., 2007). Additional evidence for this magmatic event comes from a number of reported ages of leucogranites within the Tibet (Mo et al., 2005). The abundance of leucogranitic crystallization ages between c. 55 to c. 38 Ma would suggest that these rocks form the dominant component of Gongdese granite. Notably, in samples BL-3, the 36.53 ± 0.51 Ma weighted mean of the three ages for the dark CL zircon replacing magmatic zircon can be distinguishable from the main magmatic age (Fig. 10B), based on the different zoning patterns and chemistry of these two zircon phases. The pronounced replacement structures, and marked increase in U and decrease in Th, indicate a post-magmatic, deuteric origin (Zeck et al., 2004). The very low Th/U ratios further support a metamorphic origin (Williams and Claesson, 1987; Williams, 1998; Zeck and William, 2002; Zeck et al., 2004). The age gap between magmatic zircon growth and deuteric zircon growth implies a low rate of cooling that would be typical for deep intrusion levels, or/and multi-magmatic events.

5.3.4. Earliest Oligocene syntectonic magmatism (c. 32–31 Ma)

This younger thermal event recorded within the Chongshan shear zone produced syntectonic leucogranite veins (32 ± 1.5 Ma, BL-8) and leucogranitic melts (31.52 ± 1.5 Ma, Y05-35) (Fig. 10B). The U–Pb ages from the different leucogranitic layers, along the Chongshan zone indicate that these granitic layers formed during more than one tectono-metamorphic phase. In some localities (e.g. sample site BL-8) leucogranitic melt formation is clearly associated with high-strain, strike-slip shearing under amphibolite facies conditions forcing the new melts to crystallize in layers parallel to (and slightly crosscutting) the shear-induced planar foliation (Schärer et al., 1990). After the zircons crystallized, the solidified melts were further deformed, as evidenced by development of

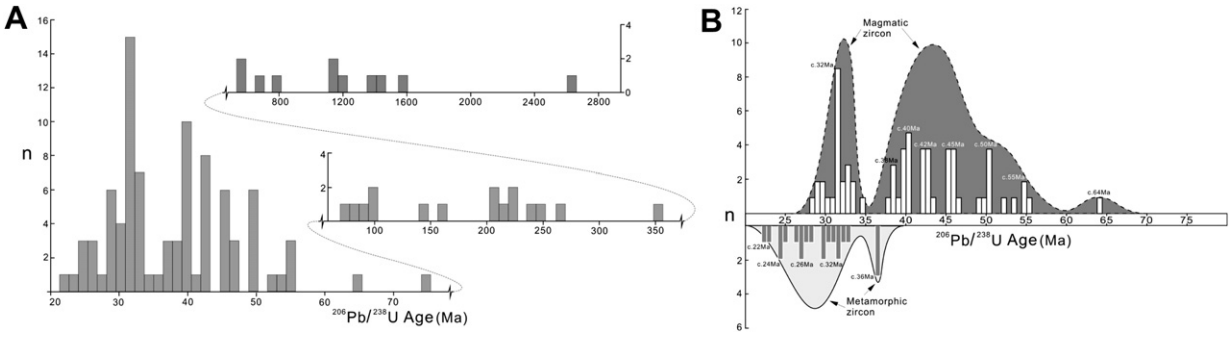

Fig. 10. Probability density curves and histograms of ^{206}Pb/^{238}U ages for granitic veins and gneisses. (A) All zircon ages groups. (B) Close-up of the four dominant age components, c. 55–38 Ma, 36 Ma, 32–31 Ma and 31–22 Ma. Noted close-up of the magmatic zircon, 32 Ma data cluster. All ages are quoted with 1σ uncertainty.

weak foliations and the sinistral strike-slip shear indicators in the melt veins. Hence, the precise ages of 32.6 ± 1.5 Ma and 31.5 ± 0.24 Ma are inferred to give a period of melt solidification that slightly predates the phase of major regional ductile deformation and strike-slip movement along the Chongshan shear zone. Recently, Akciz et al. (2008) also documented a suite of syn-teconic granites that crosscut regional fabrics and appear to be the youngest phase of igneous intrusion, accompanying the ductile strike-slip shearing along the entire Chongshan shear zone.

5.3.5. Oligocene–Miocene tectonothermal event (c. 32–22 Ma)

Considerable geochronological evidence from very thin, discontinuous rims exists to support the growth of metamorphic zircon (e.g. samples BL-1, BL-13, Y05-35 and Y05-39) during an Oligocene–earliest Miocene tectono-metamorphic reworking, that lasted from c. 32 to 22 Ma (Fig. 10B). Their very low Th/U (0.1) is consistent with a metamorphic origin (Williams and Claesson, 1987; Zeck and William, 2002; Zeck et al., 2004). These ages are in agreement with the c. 32 Ma, 26 Ma or 24 Ma U–Pb ages obtained from monazite grains within granitic veins within the Chongshan shear zone (Akciz et al., 2008). Mantles and rims formed on oscillatory zoned zircon in BL-13 and Y05-35 preserve internal zoning patterns that suggest growth under high-grade metamorphic conditions, and their ages imply a post-formation disturbance. This occurred soon after the crystallization of the granite. Thus, we suggest that one or more tectonothermal events may have affected the rocks of the Chongshan zone at some time following the intrusion of c. 32–31 Ma granitic rocks. The ages presented here may indicate that the occurrence of the syntectonic granite (e.g. granite veins for BL-8) was locally concurrent with this metamorphism that occurred at c. 32 Ma (e.g. BL-13 and Y05-39). In addition, the slight gap between syntectonic granitic occurrence along the Chongshan shear zone at c. 32 Ma and/or c. 31 Ma and the possibility for incomplete resetting of igneous zircon ages (from c. 32 to 22 Ma) during metamorphic recrystallization (e.g. the metamorphic zircons in samples BL-13, Y05-35 and Y05-39) makes it easy to reliably assign these ages to an event associated with the strike-slip shearing. Thus, it is proposed that metamorphism was associated with, or occurred soon after, strike-slip shearing along the Chongshan shear zone between c. 32 and 22 Ma. Recently, Morley (2009) has also reported c. 30 and 23 Ma magmatism and exhumation of the Mogok metamorphic belt between the Late Oligocene and Earliest Miocene.

6. ^{40}Ar/^{39}Ar thermogeochronology

In order to provide further constraints on the ages of strike-slip shear along the Chongshan shear zone, and to better understand the Cenozoic tectonics in the region, micas from deformed rocks along the shear zone were dated using the ^{40}Ar/^{39}Ar radiometric technique (see Appendix B). Analytical results are shown as age-probability diagrams and inverse isochrones in Fig. 11.

6.1. ^{40}Ar/^{39}Ar samples and results

Six samples were collected from the Chongshan shear zone for biotite and muscovite ^{40}Ar/^{39}Ar analyses. Two samples (BL-5 and BL-12) were from the deformed leucogranite veins, and samples BL-9, BL-34, B-L42 and Y05-21 were from mylonites. The veins in samples BL-5 and BL-12 were intruded along the foliation of the mylonitic gneiss, were folded and boudinaged, and indicate Tertiary shearing in this work. All these samples exhibit mylonitic foliation and stretching lineation, except for sample BL-12 which only carries a foliation only. These fabrics are defined by preferred orientation of quartz ribbons, feldspar and mica flakes. Biotites are fine-grained and indicate mid-greenschist facies conditions from 400 to 450 °C (Essene, 1989).

Feldspar deformation textures are often used as indicators for temperature during ductile deformation (Passchier and Trouw, 1996). Feldspars with plastic elongation, undulose extinction, subgrains and core-mantle structure indicate a deformation temperature of 400-500 °C (samples of BL-9, BL-34, BL-42 and Y05-21; Fig. 5B–E). Feldspars in samples BL-5 and BL-12 show both brittle fractures and plastic elongations, indicating mid-greenschist facies conditions at a temperature of c. 400 °C, together with the mineral assemblages of quartz + feldspar + biotite/muscovite. Biotite grains were separated samples BL-9, BL-12, BL-34 and BL42. Syn-kinematic muscovite came from samples BL-5 and Y05-21. The age-probability distributions for five samples (except for Y05-21) are symmetric and consistent with their inverse isochron ages (Fig. 11A–E). The age-probability of the muscovite of sample Y05-21 shows bi-peak, but the inverse isochron age approximates to its main age-probability distribution (Fig. 11F).

6.2. Analysis and interpretation of ^{40}Ar/^{39}Ar ages

^{40}Ar/^{39}Ar ages are regarded as the mineral cooling ages, which likely represent the time of syn-kinematic mineral crystallization only in cases where the deformation temperature is similar to the closure temperature of the ^{40}Ar/^{39}Ar isotopic system (Kirschner et al., 1996; Wang et al., 2006). The closure temperatures of muscovite and biotite are about 350 ± 50 °C and 300 ± 50 °C respectively (Dodson, 1973; Harrison et al., 1985; Hames and Bowring, 1994; Dunlap, 1997). The deformation temperature of these dated rocks is higher than the closure temperature of biotite. Therefore, the Argon isotopic system in biotite (BL-9, BL-12, BL-34 and BL-42) could have been totally reset and the obtained ages would therefore represent cooling

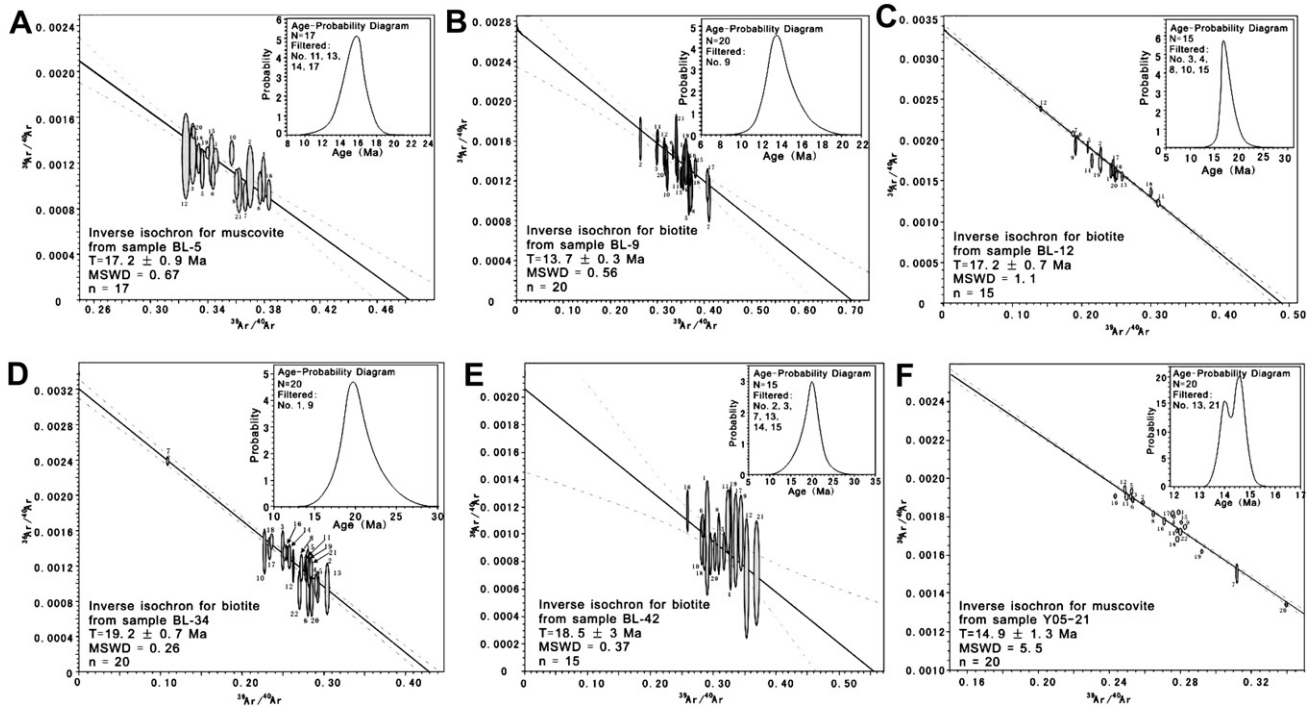

Fig. 11. $^{40}Ar/^{39}Ar$ age-probability distributions and inverse isochron diagrams with age and analytical uncertainty (1σ) for muscovite separated from the deformed leucogranitic vein sample BL-5 (A), biotite separated from the granitoid mylonite sample BL-9 (B), biotite separated from the deformed leucogranitic vein sample BL-12 (C), biotite separated from the granitoid mylonite samples BL-34 (D) and BL-42 (E), and muscovite separated from granitoid mylonite sample Y05-21 (F). See Fig. 2 for sample locations, and appendix C for analytical data.

ages after the deformation event (Zhu et al., 2005b). In contrast, the deformation temperatures of the dated samples BL5 and Y05-21 are likely close to the closure temperature of muscovite, and the cooling ages of muscovites can represent deformation ages (Lin, 2001).

It is therefore reasonable to suggest that the inverse isochron age of 17.2 ± 0.9 Ma for muscovite in BL-5 is equitable with the age of the dextral lateral shear of the Chongshan zone. Similarly, the inverse isochron age of 13.7 ± 0.3 Ma for biotite from BL-9 in the mylonite next to the BL-5 sample is regarded as the time at which the biotite cooled through its closure temperature after the dextral lateral shearing (Zhu et al., 2005b). The two cooling ages and different closure temperatures suggest a cooling rate of 14.28 °C/Ma for the northern segment of the Chongshan zone. Zircon U–Pb analysis of sample BL-5 from the deformed leucogranite yields a crystallization age of 40.13 ± 0.15 Ma. Based on these geochronological data and structural features, we suggest that the dextral strike-slip shear along the northern Chongshan shear zone, acted at c. 17 Ma, and resulted in the deformation of the Eocene granite.

The biotite inverse isochron age of 17.2 ± 0.7 Ma from the deformed leucogranite (BL-12) is suggested to be a cooling age related to sinistral strike-slip shearing in the middle segment of the zone. Zircon U–Pb analysis of sample BL-12 yields a crystallization age of 42.63 ± 0.39 Ma. The ages of 19.2 ± 0.7 Ma (BL-34) and 18.5 ± 3 Ma (BL-42) for biotite are also regarded as cooling ages. The inverse isochron age of 14.9 ± 1.3 Ma for muscovite of Y05-21 from granitic mylonite can be interpreted as a cooling age related to ongoing sinistral shear. We suggest that the difference in cooling ages can be directly related to different intensity of strike-slip generated shear heating and an inhomogeneous cooling history.

7. Tertiary transpression and strain-partition

Our findings, together with previous data, suggest that sinistral strike-slip took place synchronously along the Chongshan shear zone and Ailao Shan-Red River shear zone from the Oligocene to Miocene, overlapping the ages of folding in the Lanping-Simao terrane. The deformation along the Ailao Shan-Red River shear zone, Chongshan shear zone, and in the Lanping-Simao terrane presents a structural pattern related to transpression (Sanderson and Marchini, 1984; Dewey et al., 1998), which involves the development of contractional features such as F_1-folds, S_1 cleavages and thrusts synchronous with strike-slip shearing. The two major shear zones and conjugate strike-slip faults appear to be concordant and likely represent the ductile and brittle responses to the same regional transpression. The two conjugate ductile shear zones have their obtuse angles in the shortening direction at deep levels while conjugate brittle strike-slip faults suggest the acute angles in the shortening direction at shallow levels (Zheng et al., 2004). The traces of F_1-fold axes in the central part of the terrane have angles of 10°–20° to the foliation in the shear zones and curve into the shear zones as they approach them. Morley (2004) suggested that a transpressional setting during the Palaeogene affected a larger area from the eastern half of Thailand to the Lanping-Simao region, and that transpressional deformation located in western Thailand and Myanmar was related to motion on the Wang Chao and Three Pagodas fault zones. This setting resulted from oblique collision as India coupled with the west Burma block during the Eocene–Recent (Morley, 2009).

Based on the mapping and structural analysis of the region presented here, and inspired by the deformation model for the Shackleton Glacier area of Ross orogen (Paulsen et al., 2004), a transpression model is proposed to interpret the kinematic evolution of the region (Fig. 12). The isotopic data provide temporal constraints on the model.

The sequential development of F_1 folds, S_1 cleavage and boudinage indicates that D1 is controlled by a near E–W shortening with vertical extension (Fig. 12A). The sub-vertical foliation within the Chongshan and Ailao Shan-Red River shear zones, and flower

structure-style of the foliations across the shear zones suggest that the ductile deformed rocks once at depth have been vertically extruded along conjugate shear zones with their obtuse angle bisected in an E–W contractional direction (Woodcock and Rickards, 2003; Zheng et al., 2004). Transpression allows strike-slip and vertical extrusion to occur (Sanderson and Marchini, 1984). Fabrics in the deformed rocks show that F_2 folds, Chongshan and Ailao Shan-Red River shear zones resulted from the regional sinistral strike-slip parallel to F_1 fold axes (Fig. 12B). Asymmetric boudins parallel to the lineation in the shear zones with sinistral shear sense indicate that F_1-axis parallel (vertical) extension and sinistral shear might be coeval. Transpression is characterized by a combination of orthogonal pure shear and simple shear, commonly involving a coeval fold-normal shortening, fold-parallel extension and fold-parallel strike-slip (Jones et al., 1997; Paulsen et al., 2004). There is a marked tendency for pure- and simple-shear components to be partitioned into separate deformation domains temporally as well as spatially (Jones and Tanner, 1995; Jones et al., 1997, 2004; Lin and Jiang, 1998). As a result of such strain-partitioning, broader, weakly strained domains are typically dominated by pure shear strain components, whilst the simple shear component is localized into narrower shear zones or fault zones during progressive transpression (Tikoff and Teyssier, 1994; Jones et al., 2004; Morley, 2004). The model for the region shows that the terrane and two ductile shear zones contemporarily experienced both vertical extension and F_1-axis parallel extrusion (Fig. 12A, B). D3 is characterized by the development of conjugate brittle strike-slip faults which indicate a roughly F_1-normal shortening and F_1-parallel extension (Fig. 12C). This can be simply interpreted as that the D3 features formed near the earth surface at the end of the transpression when the deformation partition was close to 100% and simple shear component of the transpression was taken up almost entirely by slip along the major N–S trending strike slip faults, similar to the case of the San Andreas Fault (Tikoff and Teyssier, 1994; Teyssier et al., 1995). The predominance of dextral strike-slip faults was probably in response to the anisotropy produced by the previous sinistral shear (Paulsen et al., 2004).

The Chongshan shear zone, the N–S and NW–SE trending margin on the western side of the Lanping-Simao terrane forms a large-scale arcuate structure and shows opposite shear senses with the dextral N–S trending margin in the northern segment of the Chongshan zone, and the sinistral NW–SE trending margin in the middle and southern segment of the zone (Fig. 2). Given that the strike-slip shearing ages of the two segments are contemporaneous and according to the laterally unconfined transpression model suggested by Jones et al. (1997, 2004), antithetic strike-slip could be a kinematic requirement for the transpressional zone; it is not necessary to impose a separate deformational event with an opposing sense of shear (Fig. 12D) (Jones et al., 1997; Lin, 2001). Therefore, the typical structure was likely generated along the mylonitic gneiss zone during progressive transpression with strain-partitioning leading to the opposite movement senses and lateral extension of the Chongshan shear zone (Fig. 12E, F).

8. Regional significance and conclusions

Our structural and kinematic data, combined with SHRIMP, LA-ICPMS U–Pb, $^{40}Ar/^{39}Ar$ and other available geochronological data from the Chongshan shear zone, reveal a complex magmatic, metamorphic and deformational history ranging from the Triassic to Miocene.

Significant phases of magmatism along the Chongshan shear zone have occurred during Late Triassic (213 ± 5.5 Ma) and Eocene (c. 55–38 Ma). Granite vein injection, ductile strike-slip shearing and metamorphism within the Chongshan shear zone started to occur at c. 32 Ma, and may have lasted as long as c. 14 Ma, when metamorphic zircon overgrowths crystallized. These Oligocene–Miocene data indicate that shear-derived heating on the Chongshan shear zone could be responsible for the metamorphism and melting. Strike-slip shear along the Chongshan shear zone must have initiated after or at c. 32 Ma, and continued to shear after

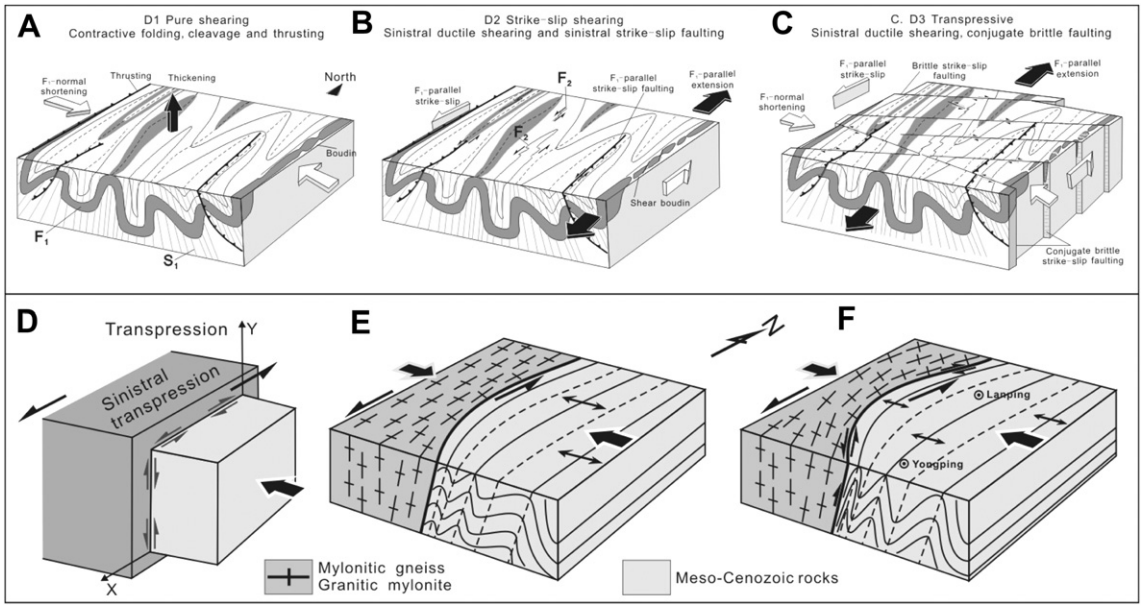

Fig. 12. Diagram showing deformation in the region between the Chongshan and Ailao Shan-Red River shear zones. (A) Regional E–W to NW–SW contraction in stage D1, producing N–S trending upright F_1 folds, cleavage S_1 and related-thrust faults. (B) Regional sinistral shearing in stage D2, generating F_2 folds and steeply plunging boudins on the limbs of F_1 folds. (C) EW-shortening in stage D3, producing conjugate strike-slip faults. (D) Transpression with lateral extrusion, shortening balanced by lateral extrusion and vertical thickening. Note that the opposite shear senses between the two edges of the Chongshan shear zone are a kinematic requirement for the extrusion along the shear direction of the three-dimension transpression (Jones et al., 1997). (E) D1 regional shortening formed F_1-folds. (F) Progressive inhomogeneous shortening during D1 and D2 reoriented the F_1-folds and formed N–S trending dextral and NW–SE trending sinistral shearing on differential segments of the Chongshan shear zone.

c. 19 or 14 Ma by which time the metamorphic rocks within the shear zone had cooled through 350 °C. Recently Wang et al. (2006) reported that strike-slip shearing on the Chongshan shear zone began by at least at c. 32 Ma based on $^{40}Ar/^{39}Ar$ dates of syn-kinematic minerals. Akciz et al. (2008) stated that strike-slip shearing continued until c. 24 Ma, and terminated at c. 17 Ma by the biotite $^{40}Ar/^{39}Ar$ ages. This previous work interpreted the $^{40}Ar/^{39}Ar$ ages as recording strike-slip shearing and uplift of the Chongshan metamorphic rocks, caused by the continued northward penetration of India into Eurasia following early Cenozoic extrusion.

During the Late Cretaceous, India northward approached the southern margin of Eurasian plate initial collision of northwestern greater India at about 65–55 Ma (Klootwijk et al., 1992; Lee and Lawver, 1995). At this time, convergence between India and Eurasia slowed down with initial thickening of the colliding continental margins. A typical change in convergence direction toward the north started to occur at the beginning of the Oligocene (c. 35 Ma) (Lee and Lawver, 1995). Although the main Indian collision occurred to the west of the Shan-Thai terrane (Mitchell, 1993), the Late Eocene metamorphism at c. 36 Ma may have resulted from crustal thickening during the early stages of that collision (Leloup et al., 1995; Wang et al., 2001; Morley, 2004), coeval with the metamorphic peak in the Karakoram terrane (Barley and Pickard, 2003; Searle et al., 2007). The Oligocene c. 31 Ma and 32 Ma leucogranites are the same age as a suite of similar syntectonic hornblende syenites, alkali granites and leucogranites that were emplaced during shear deformation along the Ailao Shan-Red River shear zone (Schärer et al., 1990; Zhang and Schärer, 1999). This magmatism overlaps in age with the Late Cretaceous-Palaeogene transpressional strain between Wang Chao-Three Pagodas fault zones in Thailand that most likely link with the Mogok metamorphic zone (Lacassin et al., 1997; Barley and Pickard, 2003; Morley, 2004, 2009; Searle et al., 2007).

Comprehensive work has been made further to the metamorphic rocks along the Mogok metamorphic zone in Burma, the NW Thailand metamorphic core complexes, and the Ailao Shan-Red River shear zone in Yunnan and North Vietnam (Morley, 2002, 2004; Searle et al., 2007). Morley (2009) stated that the c. 47–29 Ma peak metamorphism in the Mogok metamorphic zone was followed by c. 30–23 Ma magmatism and exhumation of the zone between the Late Oligocene and Earliest Miocene. Barley and Pickard (2003) also suggested that metamorphic overgrowths of zircons in the orthogneiss of Mogok metamorphic zone in Myanmar date a period of Eocene (c. 43 Ma) high-grade metamorphism possibly during crustal thickening related to the initial collision between India and Eurasia, which was followed by emplacement of syntectonic hornblende syenites and leucogranites between 35 and 23 Ma. Older Triassic metamorphic rocks are thought to have been exhumed along the Red River fault zone with regional garnet growth and metamorphism during the Oligocene–Earliest Miocene (Barley and Pickard, 2003; Gilley et al., 2003; Searle et al., 2007). Chung et al. (1997, 2005) reported that the alkali magmatic event across central Tibet, Yunnan, Laos, North Vietnam and Burma may be related more generally to the development of a very large scale Tibet-type mantle anomaly during the period 40–30 Ma. Searle (2006) insisted that these similar Eocene–Oligocene and Miocene syntectonic syenites and leucogranites that were intruded into the Ailao Shan-Red River shear zone in southwestern China and Vietnam were formed prior to sinistral lateral shearing, and that only the younger $^{40}Ar/^{39}Ar$ ages (after c. 22 Ma or probably after 16 Ma) might be related to transpressional exhumation and uplift. Considering the length and width of the Chongshan shear zone, Akciz et al. (2008) provided a possible explanation for different generations of leucogranites, which resulted from non-uniform deformation at different times, regardless of the time of their initial intrusion and crystallization. In the present work, we suggest that an important phase of localized leucogranite melting and metamorphism occurred between c. 55 and 38 Ma, and even as late as c. 36 Ma along the Chongshan shear zone and that this occurred prior to left-lateral shearing. The earliest Oligocene age of U–Pb zircon (c. 32 Ma) might indicate the onset of the strike-slip shearing, whilst the $^{40}Ar/^{39}Ar$ ages of syn-kinematic micas, ranging from c. 19 to 14 Ma, represent the main phase of strike-slip shearing along the zone. Therefore, an important Oligocene–Miocene strike-slip shearing event occurred on the Chongshan shear zone. The similar ages for magmatism, metamorphism and deformation in the Chongshan shear zone, Mogok metamorphic zone, Gaoligong shear zone, Ailao Shan-Red River shear zone and the Wang Chao and Three Pagodas fault zones, document that these zones were linked, forming a network that accommodated the northward movement of India and either rotation or expulsion of Indochina (Leloup et al., 1995; Lacassin et al., 1997; Wang and Burchfiel, 1997; Barley and Pickard, 2003; Morley, 2004, 2007; Zhang et al., 2006).

These ages from the Chongshan and Ailao Shan-Red River shear zones, together with our structural and kinematic evidence, indicate that the regions between the Gaoligong and Ailao Shan-Red River shear zones were dismembered into at least two major fragments (Lanping-Simao terrane and Shan-Thai block) that were extruded southeastward (Wang et al., 2006; Akciz et al., 2008), rather than being one single rigid block as proposed by Tapponnier et al. (1986). The contemporaneous sinistral shearing on both the Chongshan and Ailao Shan-Red River shear zones could indicate movements of the two extruded fragments relative to one another. The Tertiary sinistral transpression and extrusion are products of the oblique convergence. Thus the regional transpression was likely ultimately related to oblique plate subduction.

Acknowledgements

We are specifically grateful to Prof. Philippe H. Leloup and Prof. Ding Lin for their helpful comments and constructive criticisms that improved the original version of the manuscript. We thank Professor Wang Erqi, Xiao Wenjiao, Lin Wei, and Liu Junlai for suggestions on an earlier version of the manuscript. We are grateful to Professor Zheng Yadong and Wang Tao for thoughtful reviews and constructive critics of the manuscript. Dr. Ji Jianqing and Cai Fulong are thanked for suggestions in improving this manuscript. Dr. Qu Junfeng, Guo Lei and Qi Guowei are thanked for joining in the field work in Yunnan. The reviewer Prof. Morley Christopher and other anonymous reviewers are thanked for detailed and insightful comments and reviews. Thanks to the Editor Robert E. Holdsworth for his great support and assistance. This work was supported by the National Natural Science Foundation of China (Grant Nos. 40802050 and 40872149) and China Postdoctoral Science Foundation (No. 20070420065).

Appendix. Supplementary data

Supplementary data associated with this article can be found in the online version, at doi:10.1016/j.jsg.2010.02.001.

References

Akciz, S., Burchfiel, B.C., Crowley, J.L., Yin, J.Y., Chen, L.Z., 2008. Geometry, kinematics, and regional significance of the Chong Shan shear zone, Eastern Himalayan Syntaxis, Yunnan, China. Geosphere 4, 292–314.

Barley, M.E., Pickard, A.L., 2003. Jurassic to Miocene magmatism and metamorphism in the Mogok metamorphic belt and the India–Eurasia collision in Myanmar. Tectonics 22, 1–11.

BGMRYP (Bureau of Geology and Mineral Resources of Yunnan Province), 1990. Regional Geology of Yunnan Province. Geological Press, Beijing.
BGMRYP (Bureau of Geology and Mineral Resources of Yunnan Province), 1987. Regional geology of Yunnan Province. Geological Map 1:200,000 Sheets Lanping, Gongshan, Fugong, Bijiang, Yongping, Weixi, Dali.
Briais, A., Patriat, P., Tapponnier, P., 1993. Updated interpretation of magnetic anomalies and seefloor spreading stages in the South China Sea: implications for the Tertiary tectonics of Southeast Asia. Journal of Geophysics Research 98, 6299–6328.
Burchfiel, B.C., Wang, E.Q., 2003. Northwest-trending, middle Cenozoic, left-lateral faults in southern Yunnan, China, and their tectonic significance. Journal of Structural Geology 25, 718–792.
Chen, H., Dobson, J., Heller, F., Hao, J., 1995. Paleomagnetic evidence for clockwise rotation of the Simao region since the Cretaceous: a consequence of India–Asia collision. Earth and Planetary Science Letters 134, 203–217.
Chen, J., 1987. Ages of granitoids in western Yunnan and discussion on their isotopic datings. Yunnan Geology 6, 101–113 (in Chinese with English abstract).
Chonglakmani, C., Feng, Q., Meischner, D., Ingavat-Helmcke, R., Helmcke, D., 2001. Correlation of tectono-stratigraphic units in northern Thailand with those of western Yunnan (China). Journal of China University of Geoscience 12, 207–213.
Chung, S.L., Chu, M.F., Zhang, Y.Q., Xie, Y.W., Lo, C.H., Lee, T.Y., Lan, C.Y., Li, X.H., Zhang, Q., Wang, Y.Z., 2005. Tibetan tectonic evolution inferred from spatial and temporal variations in post-collisional magmatism. Earth Science Review 68, 173–196.
Chung, S.L., Lee, T.Y., Lo, C.H., Wang, P.L., Chen, C.Y., Yem, N.T., Hoa, T.T., Genyao, W., 1997. Intraplate extension prior to continental extrusion along the Ailaoshan-Red River shear zone. Geology 25, 311–314.
Cobbing, E.J., Mallick, D.I.J., Pitfield, P.E.F., Teoh, L.H., 1986. The granites of the Southeast Asian Tin Belt. Journal of the Geological Society, London 143, 537–550.
Dewey, J.F., Cande, S., Pitman, W.C.I., 1989. Tectonic evolution of the India–Eurasia collision zone. Eclogae Geologicae Helvetiae 82, 717–734.
Dewey, J.F., Holdsworth, R.E., Strachan, R.A., 1998. Transpression and transtension zones. Geological Society, London, Special Publications 135, 1–14.
Dodson, M.H., 1973. Closure temperature in cooling geochronological and petrological systems. Contribution Mineral Petroleum 40, 259–274.
Dong, F.L., Mo, X.X., Hou, Z.Q., Wang, Y., Bi, X.M., Zhou, S., 2005. $^{40}Ar/^{39}Ar$ ages of Himalayan alkaline rocks in Lanping basin, Yunnan Province, and their geological implications. ACTA Petrologica ET Mineralogica 24, 103–109 (in Chinese with English abstract).
Dunlap, W.J., 1997. Neocrystallisation or cooling? $^{40}Ar/^{39}Ar$ ages of white mica from low-grade mylonites. Chemical Geology 143, 181–203.
Essene, E.J., 1989. The current status of thermobarometry in metamorphic rocks. In: Daly, J.S., Cliff, R.A., Yardley, B.W. (Eds.), Evolution of Metamorphic Belts. Geological Society Special Publication 43, pp. 1–44.
Feng, Q.L., Chong, P.C., Dietrich, H., Rucha, I.H., Benpei, L., 2005. Correlation of Triassic stratigraphic between the Simao and Lampang-Phrae Basins: implications for the tectonopaleogeography of Southeast Asia. Journal of Asian Earth Sciences 24, 777–785.
Gilley, L., Harrison, T., Leloup, P.H., Ryerson, F., Lovera, O., Wang, J.H., 2003. Direct dating of left-lateral deformation along the Red River shear zone, China and Vietnam. Journal of Geophysical Research 108, 14–21.
Hames, W.E., Bowring, S.A., 1994. An empirical evaluation of the argon diffusion geometry in muscovite. Earth and Planetary Science Letters 124, 161–167.
Harrison, T.M., Duncan, I., McDougall, I., 1985. Diffusion of ^{40}Ar in biotite: temperature, pressure and compositional effects. Geochimica et Cosmochimica Acta 49, 2461–2468.
Heppe, K., Helmcke, D., Wemmer, K., 2007. The Lancang River Zone of southwestern Yunnan, China: A questionable location for the active continental margin of Paleotethys. Journal of Asian Earth Sciences 30, 706–720.
Hoskin, P.W.O., Black, L.P., 2000. Metamorphic zircon formation by solid state recrystallisation of protolith igneous zircon. Journal of Metamorphic Geology 18, 423–439.
Ji, J.Q., Zhong, D.L., Zhang, L.S., 2000. Kinematics and dating of Cenozoic strike-slip faults in the Tengchong area, west Yunnan: implications for the block movement in the southeastern Tibet Plateau. Chinese Journal of Geology 35, 336–349 (in Chinese with English abstract).
Jolivet, L., Beyssac, O., Goffe, B., Avigad, D., Lepvrier, C., Maluski, H., Thang, T.T., 2001. Oligo-Miocene midcrustal subhorizontal shear zone in Indochina. Tectonics 20, 46–57.
Jones, R.R., Holdsworth, R.E., Bailey, W., 1997. Lateral extrusion in transpression zones: the importance of boundary conditions. Journal of Structural Geology 19, 1201–1217.
Jones, R.R., Holdsworth, R.E., Clegg, P., McCaffrey, K., Tavarnelli, E., 2004. Inclined transpression. Journal of Structural Geology 26, 1531–1548.
Jones, R.R., Tanner, P.W.G., 1995. Strain partitioning in transpression zones. Journal of Structural Geology 17, 793–802.
Kirschner, L., Cosca, M.A., Masson, H., Hunziker, J.C., 1996. Staircase $^{40}Ar/^{39}Ar$ spectra of fine-grained white mica: timing and duration of deformation and empirical constraints on argon diffusion. Geology 24, 747–750.
Klootwijk, C.T., Gee, J.S., Peirce, J.W., Smith, G.M., McFadden, P.L., 1992. An early India–Asia contact: paleomagnetic constraints from Ninetyeast Ridge, ODP Leg 121. Geology 20, 395–398.
Lacassin, R., Maluski, H., Leloup, P.H., Tapponnier, P., Hinthong, C., Siribhakdi, K., Chuaviroi, S., Charoenravat, A., 1997. Tertiary diachronic extrusion and deformation of western Indochina: structural and $^{40}Ar–^{39}Ar$ evidence from NW Thailand. Journal of Geophysical Research 102, 10013–10037.
Lee, T.Y., Lawver, L.A., 1995. Cenozoic plate reconstruction of Southeast Asia. Tectonophysics 251, 85–138.
Leloup, P.H., Arnaud, N., Lacassin, R., Kienast, J., Harrison, T., Trinh, P., Replumaz, A., Tapponnier, P., 2001. New constraints on the structure, thermochronology and timing of the Ailao Shan-Red River shear zone SE Asia. Journal of Geophysical Research 106, 6683–6732.
Leloup, P.H., Kienast, J.R., 1993. High-temperature metamorphism in a major strike-slip shear zone: the Ailao Shan-Red River, People's Republic of China. Earth and Planetary Science Letters 118, 213–234.
Leloup, P.H., Lacassin, R., Tapponnier, P., Schärer, U., Zhong, D.L., Liu, X.H., Zhang, L.S., Ji, S.C., Phan, T., 1995. The Ailao Shan-Red River shear zone (Yunnan, China), Tertiary transform boundary of Indochina. Tectonophysics 251, 3–84.
Leloup, P.H., Tapponnier, P., Lacassin, R., 2007. Discussion on the role of the Red River shear zone, Yunnan and Vietnam, in the continental extrusion of SE Asia. Journal of the Geological Society, London 164, 1253–1260.
Lin, S.F., 2001. $^{40}Ar/^{39}Ar$ age pattern associated with differential uplift along the Eastern highlands shear zone, Cape Breton Island, Canadian Appalachians. Journal of Structural Geology 23, 1031–1042.
Lin, S.F., Jiang, D.Z., 1998. Transpression (or transtension) zones of triclinic symmetry: natural example and theoretical modeling. In: Holdsworth, R.E., Strachran, R.A., Dewey, J.F. (Eds.), Continental Transpressional and Transtensional Tectonics. Geological Society of London, Special Publication 135, pp. 41–57.
Lin, T.H., Lo, C.H., Chung, S.L., Hsu, F.J., Yeh, M.W., Lee, T.Y., Ji, J.Q., Wang, Y.Z., Liu, D.Y., 2009. $^{40}Ar/^{39}Ar$ dating of the Jiali and Gaoligong shear zones: Implications for crustal deformation around the Eastern Himalayan Syntaxis. Journal of Asian Earth Sciences 34, 674–685.
Liu, C., Zhu, J., Xu, X., 1989. The Hercynian collision type granites of West Yunnan and their tectonic significance. Journal of Southeast Asia Earth Science 3, 263–270.
Ludwig, K.R., 2003. Isoplot 3.00 A geochronological took it for Microsoft Excel. In: Special Publications 4. Berkeley Geochronological Center, Berkeley, CA, 71 pp.
Meng, W.Y., Tung, Y.L., Ching, H.L., Sun, L.C., Ching, Y.L., Tran, T.A., 2008. Structural evolution of the Day Nui Con Voi metamorphic complex: implications on the development of the Red River Shear Zone, Northern Vietnam. Journal of Structural Geology 30, 1540–1553.
Metcalfe, I., 2006. Paleozoic and Mesozoic tectonic evolution and palaeogeography of East Asian crustal fragments: The Korean Peninsula in context. Gondwana Research 9, 24–46.
Metcalfe, I., Sone, M., 2008. Biostratigraphy and palaeobiogeography of Lower Permian (lower Kungurian) conodonts from the Tak Fa Formation (Saraburi Limestone), Thailand. Palaeogeography, Palaeoclimatology, Palaeoecology 257, 139–151.
Mo, X.X., Dong, G.C., Zhao, Z.D., 2005. Timing of magma mixing in the Gangdise magmatic belt during the India-Asia collision: zircon SHRIMP U-Pb dating. Acta Geologica Sinica (English Edition) 79, 66–76.
Morley, C.K., 2002. A tectonic model for the Tertiary evolution of strike-slip faults and rift basins in SE Asia. Tectonophysics 347, 189–215.
Morley, C.K., Woganan, N., Sankumarn, N., Hoon, T.B., Alief, A., Simmons, M., 2001. Late Oligocene – recent stress evolution in rift basins of Northern and Central Thailand: implications for escape tectonics. Tectonophysics 334, 115–150.
Morley, C.K., 2004. Nested strike-slip duplexes, and other evidence for Late Cretaceous–Palaeogene transpressional tectonics before and during India–Eurasia collision, in Thailand, Myanmar and Malaysia. Journal of the Geological Society, London 161, 799–812.
Morley, C.K., 2007. Variations in Late Cenozoic – recent strike-slip and oblique-extensional geometries, within Indochina: the influence of pre-existing fabrics. Journal of Structural Geology 29, 36–58.
Morley, C.K., 2009. Evolution from an oblique subduction back-arc mobile belt to a highly oblique collisional margin: the Cenozoic tectonic development of Thailand and eastern Myanmar. In: Geological Society of London, Special Publications 318 373–403.
Mitchell, A.G.H., 1993. Cretaceous–Cenozoic tectonic events in the Western Myanmar (Burma)–Assam region. Journal of the Geological Society, London 150, 1089–1102.
Passchier, C.W., Trouw, R.A.J., 1996. Microtectonics. Springer, 289 pp.
Paulsen, T.S., Encarnacion, J., Grunow, A.M., 2004. Structure and timing of transpressional deformation in the Shackleton Glacier area, Ross orogen, Antarctica. Journal of the Geological Society, London 161, 1027–1038.
Peltzer, G., Tapponnier, P., 1988. Formation and evolution of strike-slip faults, rifts, and basins during India–Asia collision: an experimental approach. Journal of Geophysical Research 93, 85–117.
Peng, T.P., Wang, Y.J., Zhao, G.C., Fan, W.M., Peng, B.X., 2008. Arc-like-volcanic rocks from the southern Lancangjiang zone, SW China: geochronological and geochemical constraints on their petrogenesis and tectonic implications. Lithos 102, 358–373.
Ring, U., Collins, A.S., 2005. U–Pb SIMS dating of synkinematic granites: timing of core-complex formation in the northern Anatolide belt of western Turkey. Journal of the Geological Society, London 162, 289–298.
Sanderson, D.J., Marchini, W.D., 1984. Transpression. Journal of Structural Geology 6, 449–458.

Schärer, U., Tapponnier, P., Lacassin, R., Leloup, P.H., Zhong, D.L., Ji, S.C., 1990. Intraplate tectonics in Asia: a precise age for large-scale Miocene movement along the Ailao Shan-Red River shear, China. Earth and Planetary Science Letters 97, 65–77.

Searle, M.P., 2006. Role of the Red River Shear zone, Yunnan and Vietnam, in the continental extrusion of SE Asia. Journal of the Geological Society 163, 1025–1036.

Searle, M.P., Noble, S.R., Cottle, J.M., Waters, D.J., Mitchell, A.H.G., Hlaing, T., 2007. Tectonic evolution of the Mogok metamorphic belt, Burma (Myanmar) constrained by U–Th–Pb dating of metamorphic and magmatic rocks. Tectonics 26, 1–24.

Socquet, A., Pubellier, M., 2005. Cenozoic deformation in western Yunnan (China–Myanmar border). Journal of Asian Earth Sciences 24, 495–515.

Tapponnier, P., Lacassin, R., Leloup, P.H., Schärer, U., Zhong, D.L., Liu, X.H., Ji, S.C., Zhang, L.S., Zhong, J., 1990. The Ailao Shan-Red River Metamorphic belt: tertiary left lateral shear between Sundaland and South China. Nature 343, 431–437.

Tapponnier, P., Peltzer, G., Armijo, P., 1986. On the mechanics of the collision between India and Asia. In: Coward, M.P., Ries, A.C. (Eds.), Collision Tectonics. Geological Society, London, Special Publication 19, pp. 115–157.

Tapponnier, P., Peltzer, G., Le Dain, A.Y., Armijo, R., Cobbold, P., 1982. Propagating extrusion tectonics in Asia: new insights from simple experiments with plasticine. Geology 10, 611–616.

Teyssier, C., Tikoff, B., Markley, M., 1995. Oblique plate motion and continental tectonics. Geology 23, 447–450.

Tikoff, B., Teyssier, C., 1994. Strain modeling of displacement-field partitioning in transpressional orogens. Journal of Structural Geology 16, 1575–1588.

Vavra, G., Gebauer, D., Schmid, R., Compston, W., 1996. Multiple zircon growth and recrystallisation during polyphase Late Carboniferous to Triassic metamorphism in granulites of Ivrea Zone (Southern Alps): an ion microprobe (SHRIMP) study. Contributions to Mineralogy and Petrology 122, 337–358.

Vavra, G., Schmidt, R., Gebauer, D., 1999. Internal morphology, habit and U–Th–Pb microanalysis of amphibolite to granulite facies zircons: geochronology of the Ivrea zone (Southern Alps). Contributions to Mineralogy and Petrology 134, 380–404.

Wang, E.Q., Burchfiel, B.C., 1997. Interpretation of Cenozoic tectonics in the right-lateral accommodation zone between the Ailao Shan Shear Zone and the Eastern Himalayan Syntaxis. International Geology Review 39, 191–219.

Wang, J.H., Yin, A., Harrison, T.M., Grove, M., Zhang, Y.Q., Xie, G.H., 2001. A tectonic model for Cenozoic igneous activities in the eastern Indo-Asian collision zone. Earth and Planetary Science Letters 188, 123–133.

Wang, Y.J., Fan, W.M., Zhang, Y.H., Peng, T.P., Chen, X.Y., Xu, Y.G., 2006. Kinematics and $^{40}Ar/^{39}Ar$ geochronology of the Gaoligong and Chongshan shear systems, western Yunnan, China: implications for early Oligocene tectonic extrusion of SE Asia. Tectonophysics 418, 235–254.

Wilcox, R.E., Harding, T.P., Seely, D.R., 1973. Basic wrench tectonics. American Association of Petroleum Geologists Bulletin 57, 74–96.

Williams, I.S., 1998. U–Th–Pb geochronology by ion microprobe. In: Mckibben, M.A., Shanks, W.C., Ridley, W.C., Ridley, W.I. (Eds.), Applications of Microanalytical Techniques to Understanding Mineralizing Processes. Reviews in Economic Geology 7, 1–35.

Williams, I.S., Claesson, S., 1987. Isotopic evidence for the Precambrian provenance and Caledonian metamorphism of high grade paragneisses from the Seve Nappes, Scandinavian Caledonides; II, ion microprobe zircon U–Th––Pb. Contributions to Mineralogy and Petrology 97, 205–217.

Woodcock, N.H., Fischer, M., 1986. Strike-slip duplexes. Journal of Structural Geology 8, 725–735.

Woodcock, N.H., Rickards, B., 2003. Transpressive duplex and flower structures: dent fault system, NW England. Journal of Structural Geology 25, 1981–1992.

Xue, C.J., Chen, Y.C., Wang, D.H., Yang, J.M., Yang, W.G., Zeng, R., 2003. Geology and isotopic composition of helium, neon, xenon, and metallogenic age of the Jinding and Baiyangping ore deposits, northwest Yunnan, China. Sciences in China (series D) 46, 789–800.

Zeck, H.P., Whitehouse, M.J., 2002. Repeated age resetting in zircon from Hercynian-Alpine polymetamorphic schists (Betic-Rif tectonic belt, S Spain) – a U–Th–Pb ion microprobe study. Chemical Geology 182, 275–292.

Zeck, H.P., William, I.S., 2002. Inherited and magmatic zircon from Neogene Hoyazo cordierite dacite, SE Spain-anatectic source rock provenance and magmatic evolution. Journal of Petrology 43, 1089–1104.

Zeck, H.P., Wingate, M.T.D., Pooley, G.D., Ugidos, J.M., 2004. A sequence of Pan-African and Hercynian events recorded in zircons from an orthogneiss from the Hercynian Belt of western central Iberia – an ion microprobe U–Pb study. Journal of Petrology 45, 1613–1629.

Zhang, J.J., Zhong, D.L., Sang, H.Q., Zhou, Y., 2006. Structural and geochronological evidence for multiple episodes of tertiary deformation along the AilaoShan-Red River shear zone, Southeastern Asia, since the Paleocene. ACTA Geologica Sinica (English Edition) 80, 79–96.

Zhang, L.S., Schärer, U., 1999. Age and origin of magmatism along the Cenozoic Red River shear belt, China. Contributions to Mineralogy and Petrology 134, 67–85.

Zhang, R., Cong, B., Maruyama, S., Liou, J.G., 1993. Metamorphism and tectonic evolution of the Lancang paired metamorphic belts, southwestern China. Journal of Metamorphic Geology 11, 605–619.

Zheng, Y.D., Wang, T., Ma, M.B., Davis, G.A., 2004. Maximum effective moment criterion and the origin of low-angle normal faults. Journal of Structural Geology 26, 271–285.

Zhong, D.L., 2000. Paleotethyan Orogenic Belts in Yunnan and Western Sichuan. Science Press, Beijing. pp. 230–240.

Zhong, D.L., Tapponnier, P., 1990. Large-scale strike slip fault: the major structure of intracontinental deformation after collision. Chinese Science Bulletin 35, 304–309.

Zhu, B., William, S.F.K., David, B.R., Brian, S.C., Naseer, S., 2005a. Age of initiation of the India-Asia Collision in the East-Central Himalaya. Journal of Geology 113, 265–285.

Zhu, G., Wang, Y.S., Liu, G.S., Niu, M.L., Xie, C.L., Li, C.C., 2005b. $^{40}Ar/^{39}Ar$ dating of strike-slip motion on the Tan-Lu fault zone, East China. Journal of Structural Geology 27, 1379–1398.